Contents lists available at ScienceDirect

Arabian Journal of Chemistry

journal homepage: www.ksu.edu.sa

Boosting biodiesel production of waste frying oil using solid magnetic acid catalyst from agro-industrial waste

Matheus Arrais Gonçalves [a], Hiarla Cristina Lima dos Santos [a], Thaissa Saraiva Ribeiro [a], Alexandre da Cas Viegas [b], Geraldo Narciso da Rocha Filho [a], Leyvison Rafael Vieira da Conceição [a,*]

[a] Federal University of Pará, Institute of Exact and Natural Sciences, Graduate in Chemistry Program, Laboratory of Catalysis and Oleochemical, 66075–110 Belém, Pará, Brazil
[b] Federal University of Rio Grande do Sul, Institute of Physics, 90035–190 Porto Alegre, Rio Grande do Sul, Brazil

ARTICLE INFO

Keywords:
Biodiesel
Magnetic catalyst
Cobalt ferrite
Rice husk ash
Molybdenum oxide
Transesterification reaction

ABSTRACT

In the present study, a new magnetic acid solid catalyst composed of an agro-industrial waste (rice husk ash-RHA) magnetized with cobalt ferrite ($CoFe_2O_4$) and impregnated with MoO_3 was synthesized and applied in the methyl transesterification reaction of waste frying oil (WFO) for biodiesel production. The catalyst was synthesized by wet impregnation method and characterized by the following techniques: surface acidity, X-ray diffraction (XRD), Fourier transform infrared spectroscopy (FTIR), scanning electron microscopy (SEM), energy dispersion X-ray spectroscopy (EDS), and vibrating sample magnetometer (VSM). The one variable at time (OVAT) technique was used to optimize the variables of the transesterification reaction in the following ranges: temperature (130.0–170.0 °C), methanol:oil molar ratio (10:1–50:1), catalyst amount (2.0–10.0 wt%), and reaction time (1.0–5.0 h). The results demonstrate that the application of the MoO_3/RHA-$CoFe_2O_4$ synthesized catalyst resulted in the attainment a biodiesel with ester content of 94.6 % under the optimized reaction conditions: temperature of 160.0 °C, methanol:oil molar ratio of 20:1, catalyst amount of 6.0 wt%, and reaction time of 3.0 h. The biodiesel produced was characterized and presented physicochemical properties in accordance with the limits established by the international standards ASTM D6751 and EN 14214. The kinetic study of the transesterification process revealed that the pseudo-first order model is the most suitable with an activation energy of 27.3 kJ mol^{-1}. In addition, the catalyst showed bifunctional character (catalytic and magnetic), as well as high catalytic stability after ten reaction cycles, maintaining the production of biodiesel with ester content above 70.0 %, indicating its high potential for development and application.

1. Introduction

Biodiesel, defined as alkyl esters, has been attracting attention as a renewable biofuel since it emerges as a clean energy alternative of great potential due to the fact that it is obtained from the conversion of biomass and has characteristics similar to petroleum diesel oil (Erison et al., 2022; Kiehbadroudinezhad et al., 2023; Lima et al., 2017). Biodiesel can be produced by several routes, with the main one being the transesterification reaction, consisting of the reaction of a short chain alcohol with triglyceride source to obtain esters (biodiesel) and glycerol as co-product (Kiehbadroudinezhad et al., 2023; Abdullahi et al., 2023).

One way to reduce the costs generated in the biodiesel production process is the use of residual raw materials, with low added value, such as waste frying oil (WFO), which is widely studied due to its abundance (Ulakpa et al., 2022; Adhikesavan et al., 2022). In addition, many pieces of research have been carried out for the development of heterogeneous catalysts from waste materials in order to be applied in the production of biodiesel, since heterogeneous catalysts have advantages over homogeneous catalysts (more used industrially) due to the possibility of being reused in the reaction process and not causing operational problems related to corrosion (Mares et al., 2021; Conceição et al., 2017).

Among the various types of heterogeneous catalysts applied to biodiesel production reported in the literature, heteropolyacids (Gonçalves et al., 2021a; Conceição et al., 2019), zeolites (Mohebbi et al., 2020; Zhang et al., 2022), sulfonated carbons (Bastos et al., 2020; Correa et al., 2020; Correa et al., 2023), magnetic materials (Krishnan et al., 2021; Xie

* Corresponding author.
E-mail address: rafaelvieira@ufpa.br (L.R. Vieira da Conceição).

https://doi.org/10.1016/j.arabjc.2023.105521
Received 29 August 2023; Accepted 3 December 2023
Available online 5 December 2023

and Li, 2023), agro-industrial tailings (Moayedi et al., 2019), as well as supported catalysts, consisting of an active phase impregnated in a catalytic support of high stability and high surface area (Conceição et al., 2017; Conceição et al., 2019), stand out. In this context, rice husk ash (RHA), an agro-industrial waste, produced from the burning of rice husk, has been studied as an alternative to be used as a catalytic support because of its richness in silica (content > 85.0 %, SiO_2) and its high availability, with about 70.0 million tonnes of RHA produced annually (Moayedi et al., 2019; Chen et al., 2013). RHA can be widely used as adsorbents, biochar, fertilizers in the concrete industry, and as catalysts (Moayedi et al., 2019). In the study reported by Chen et al. (2015), the authors investigated the application of the catalyst composed of lithium carbonate (Li_2CO_3) impregnated in RHA in the production of biodiesel and obtained a biofuel with conversion into esters of 99.5 %, under the reaction conditions: temperature of 65 °C, reaction time of 3 h, catalyst amount of 4 wt%, and methanol:oil molar ratio of 24:1.

In addition, it is worth mentioning that, among the heterogeneous catalysts applied to biodiesel production, alternatives have been studied that make it possible to reduce the cost of production by facilitating the separation of the catalytic solid using a magnetic field, which would dispense with the use of energy in traditionally used separation media, such as centrifugation and filtration (Krishnan et al., 2021). In this sense, several bifunctional catalysts have been reported in the literature, especially those composed of magnetic materials, such as ferrites of MFe_2O_4 structure, M being a metal, impregnated with metal oxides as the active phase.

In the study reported by Gonçalves et al., (2021b), the application of a catalyst composed of molybdenum oxide (MoO_3) impregnated in strontium ferrite ($SrFe_2O_4$) in the production of biodiesel was studied. The results achieved by the authors demonstrate the attainment of a biofuel with ester content of 95.4 %, under the reaction conditions: temperature of 164.0 °C, reaction time of 4.0 h, catalyst amount of 10.0 wt%, and methanol:oil molar ratio of 40:1. In the study reported by Foroutan et al. (2022), the authors investigated the application of a catalyst consisting of potassium carbonate (K_2CO_3) impregnated in chalk oxide magnetized with cobalt ferrite ($CoFe_2O_4$) in the production of biodiesel and obtained a biofuel with conversion to esters of 99.27 %, under the following reaction conditions: temperature of 80.0 °C, reaction time of 2.95 h, catalyst amount of 2.65 wt%, and methanol:oil molar ratio of 15.2:1.

Therefore, the present study aims to synthesize and characterize a new magnetic acid solid catalyst composed of molybdenum oxide (MoO_3) impregnated in RHA magnetized with $CoFe_2O_4$ for application in the methyl transesterification reaction of WFO to produce high ester biodiesel.

2. Methodology

2.1. Materials

The RHA was acquired from a local rice production cooperative (Bélem, Pará, Brazil). Iron (III) chloride ($FeCl_3$, 99.8 %) and cobalt nitrate ($Co(NO_3)_2{\cdot}6H_2O$, 99.8 %) were aquired from Sigma-Aldrich and ECIBRA, respectively. The methyl hetadecanoate (99.0 %, $C_{18}H_{36}O_2$) was purchased from Sigma-Aldrich, while nitric acid (37.0 % HNO_3), ethyl alcohol (99.8 %, C_2H_6O), and methyl alcohol (99.8 %, CH_3OH) were acquired from Vetec. Ammonium heptamolybdate ($(NH_4)_6Mo_7O_{24}$ $4{\cdot}H_2O$) and sodium hydroxide (97.0 %, NaOH) were aquired from Dinamica. In addition, heptane (99.0 %, C_7H_{16}) and hexane (99.0 %, C_6H_{14}) were purchased from Êxodo. All materials listed for the development of this study were used without prior treatment. The WFO used as feedstock for biodiesel production was purchased from a local market. The physicochemical properties of WFO are shown in Table 1.

Table 1
Physicochemical properties of WFO used to produce biodiesel.

Properties	Value
Acid value, (mg KOH g^{-1}) (AOCS Cd 3d–63)	2.2
Saponification value, (mg KOH g^{-1}) (AOCS Tl 1a–64)	186.3
Viscosity at 40 °C, (mm^2 s^{-1})	36.4
Moisture content, (%) (AOCS Ca 2b–38)	0.1
Molecular weight, (g/mol)	855

2.2. Preparation of heterogeneous acid magnetic catalyst (MoO_3/RHA-$CoFe_2O_4$)

2.2.1. Synthesis of cobalt ferrite ($CoFe_2O_4$)

Cobalt ferrite was synthesized by coprecipitation method, according to the methodology adopted by Tamjidi et al. (2022), with adaptations. The synthesis process consisted of four steps, in which Step 1 was done by mixing in 100.0 mL of water from $Co(NO_3)_2{\cdot}6H_2O$ and $FeCl_3$ in a Fe: Co = 2 M ratio, followed by the addition of HNO_3 to pH = 3 and subsequent addition of NaOH (4.0 mol/L) to promote precipitation at pH = 12. Then, the system was kept under mechanical agitation and heating at 80.0 °C for 4.0 h. Step 2 consisted of the filtration procedure, while Step 3 was completed by washing the precipitated solid obtained until the washing water reached pH = 7, followed by drying the material in an oven at 80.0 °C for 12.0 h. Finally, in Step 4, the material was calcined at 800.0 °C for 3.0 h in order to obtain the $CoFe_2O_4$, as shown in Fig. 1(a).

2.2.2. Magnetic catalyst synthesis (MoO_3/RHA-$CoFe_2O_4$)

The MoO_3/RHA-$CoFe_2O_4$ catalyst was prepared by the wet impregnation method according to the methodology adopted by Dos Santos et al. (2022), as shown in Fig. 1(b). First, in the impregnation step (Step 1), 1.0 g of RHA and an amount of $CoFe_2O_4$ corresponding to 30.0 % of the mass of RHA were added to a beaker containing 40.0 mL of water. Then, a certain amount of $(NH_4)_6Mo_7O_{24}$ $4{\cdot}H_2O$ was added in order to obtain catalysts with molybdenum metal contents of 10.0, 20.0, 30.0, and 40.0 %, followed by the maintenance of the mixture under mechanical stirring for 3.0 h at room temperature. Subsequently, in Step 2, the material was dried in an oven at 80.0 °C for 12.0 h, and, finally, in Step 3, the material was calcined at 450.0 °C for 2.0 h, in order to obtain the catalyst *x*-MoO_3/RHA-$CoFe_2O_4$, in which *x* corresponds to the content of impregnated molybdenum metal.

2.3. Materials characterization techniques

The surface acidity of $CoFe_2O_4$, RHA, and MoO_3/RHA-$CoFe_2O_4$ materials were determined according to the methodology developed by Boehm (1994), with adaptations. In this method, 0.1 g of the sample was suspended in a solution of NaOH (0.1 mol/L) and stirred at 25.0 °C for 24.0 h. Then the sample is magnetically separated and the supernatant was titrated with a solution of HCl (0.1 mol/L), using phenolphthalein as an indicator.

The X-ray diffractograms (XRD) of MoO_3, $CoFe_2O_4$, RHA, and MoO_3/RHA-$CoFe_2O_4$ were obtained in a BRUKER diffractometer, model D8 ADVANCE. The scan interval was $20° < 2\theta < 90°$, with angular pitch of 0.02° and time per step of 0.01 s. In addition, the radiation used was Cu Kα (1.541874 Å) with 40 KV and 30 mA. The Fourier transform infrared spectroscopy (FTIR) analysis was performed in order to qualitatively investigate the functional groups present in the MoO $_3$, $CoFe_2O_4$, RHA, and MoO_3/RHA-$CoFe_2O_4$ materials, using a BRUKER spectrometer, model Verterx 70 V, with analysis in the spectral range of 2000–400.0 cm^{-1}, 4.0 cm^{-1} resolution and 32 sweeps.

The surface morphology of MoO_3, $CoFe_2O_4$, RHA, and MoO_3/RHA-$CoFe_2O_4$ was analyzed by scanning electron microscopy (SEM) using a Vega 3 LMU TESCAN microscope. The analysis of the surface elemental composition of MoO_3, $CoFe_2O_4$, RHA, and MoO_3/RHA-$CoFe_2O_4$ was performed by energy dispersion X-ray spectroscopy (EDS) using an

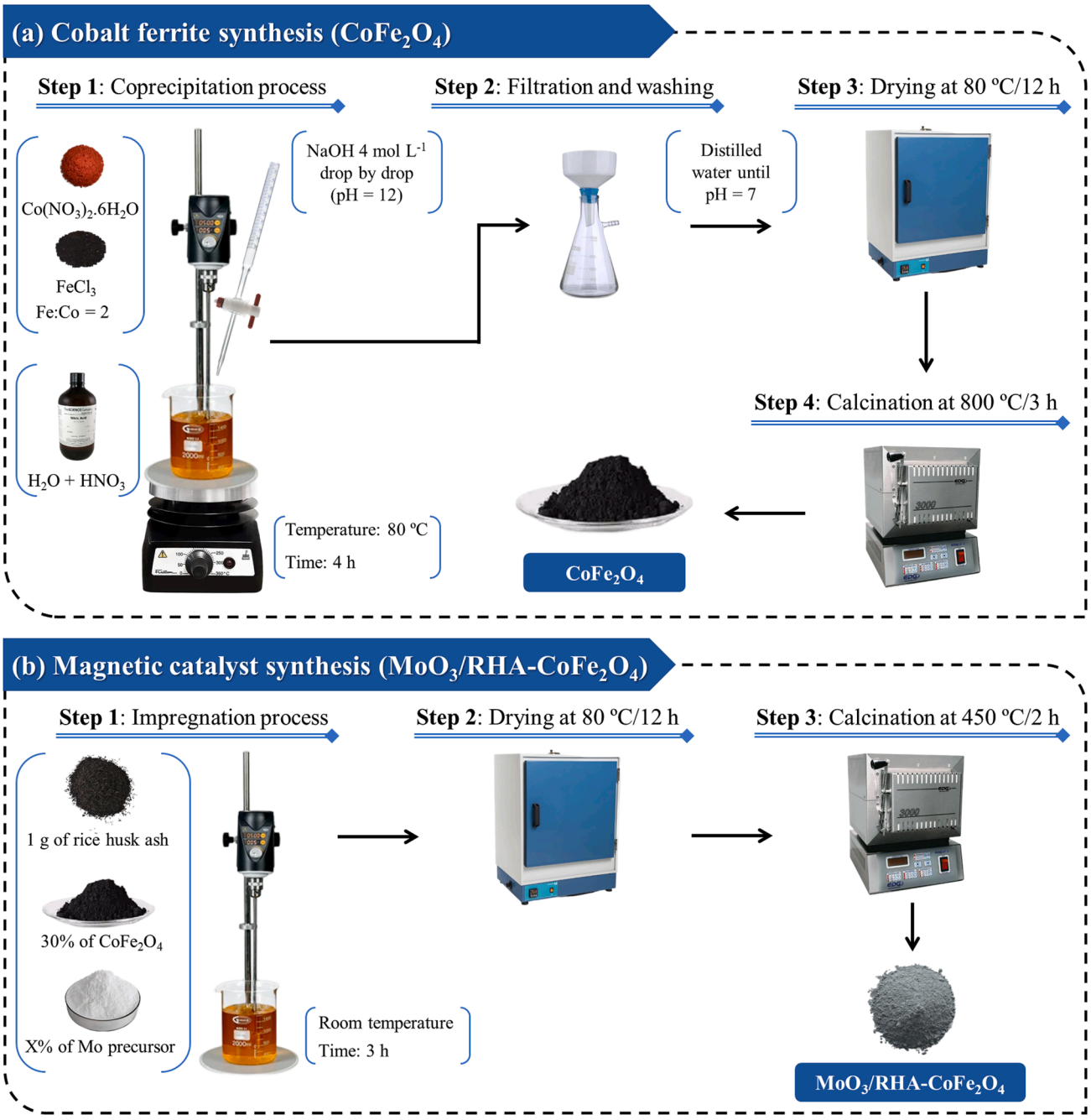

Fig. 1. Schematic diagram of (a) $CoFe_2O_4$ and (b) MoO_3/RHA-$CoFe_2O_4$ synthesis.

Oxford Microanalysis system®, Aztec Energy X-Act model, with 129 eV resolution. Finally, the magnetic properties of $CoFe_2O_4$ and MoO_3/RHA-$CoFe_2O_4$ were evaluated by the technique of vibrating sample magnetometer (VSM), model Microsense magnetometer EZ9, with application of a magnetic field in the range of −20000.0 Oersted (Oe) to 20000.0 Oe, at room temperature.

2.4. Catalytic tests

In the catalytic tests, WFO, methanol, and the MoO_3/RHA-$CoFe_2O_4$ synthesized catalyst were used as reagents. The transesterification reactions were performed in a PARR 5000 series pressurized reactor, with constant stirring at 900 RPM. Initially, the influence of molybdenum content (10.0, 20.0, 30.0 and 40.0 %) in the final composition of the catalyst as a function of its performance in the synthesis of biodiesel was studied. Subsequently, after the selection of the catalyst with the best performance, the parameters of the transesterification reaction using the one variable at time (OVAT) technique in the following intervals: reaction temperature (130.0–170.0 °C), WFO:methanol molar ratio (10:1–50:1), catalyst amount (2.0–10.0 wt%), and reaction time (1.0–5.0 h) were studied. All ranges studied were defined in preliminary tests. In addition, the catalytic performance using only RHA and $CoFe_2O_4$ materials (blank reactions) in the reaction medium were also evaluated.

At the end of each catalytic test, the products obtained were separated from the catalyst magnetically and washed with 500.0 mL of distilled water at 80.0 °C to remove impurities such as unreacted methanol, glycerol residues, mono -, di -, and triacylglycerols. Then, the biodiesel sample was dried in an oven at 60.0 °C for 24.0 h and stored for subsequent determination of the ester content by gas chromatography

(GC).

2.5. Determination of biodiesel properties

The biodiesels obtained in the catalytic tests were analyzed for their ester content by GC according to the methodology adapted from the European standard EN 14103 described by Dos Santos et al. (2022). The Varian gas chromatograph, model CP-3800, equipped with flame ionization detector (FID) and CP WAX 52 CB (30.0 m long, 0.32 mm diameter and 0.25 μm film) capillary column was used. Helium gas was used as a mobile phase with a flow of 1.0 mL min^{-1} and initial oven temperature programming of 170.0 °C, with heating rate of 10.0 °C min^{-1} up to 250.0 °C (same temperature as FID and injector). Heptane was used as a solvent, methyl heptadecanoate as internal standard and the injection volume was of 1.0 μL. The ester content (EC) was calculated according to Eq. (1):

$$EC\,(\%) = \frac{(\sum A_T) - A_{IS}}{A_{IS}} \times \frac{C_{IS}}{C_{B100}} \times 100 \quad (1)$$

where: $\sum A_T$ is the sum of the total area of the peaks; A_{IS} is the area of the peaks of the internal standard; C_{IS} is the concentration of the solution of the internal standard (mg L^{-1}); C_{B100} is the concentration of biodiesel after dilution (mg L^{-1}).

2.6. Catalyst reuse study

At the end of the transesterification reaction, the MoO_3/RHA-$CoFe_2O_4$ catalyst recovered by application of the magnetic field, was washed three times with 30.0 mL of hexane and 20.0 mL of ethanol to remove impurities. Then, the catalyst was dried in an oven at 80.0 °C for a period of 12.0 h and re-employed in the catalytic tests in order to evaluate its catalytic stability in the reactional cycles.

3. Results and discussion

3.1. Influence of molybdenum concentration

The influence of the active phase on the final composition of the catalyst is of paramount importance when studying supported catalysts, since it is aimed at obtaining a high performance catalytic solid from the use of the least amount of active phase impregnated in a support when compared with the use of mass catalysts, which weights on the final cost of the catalyst and the process as a whole (Mehrabadi et al., 2017). In this respect, the influence of the concentration of 10.0, 20.0, 30.0, and 40.0 % molybdenum (active phase) in relation to the ester content of biodiesels obtained in catalytic tests was studied, as shown in Fig. 2. The reactions were performed under the following non-optimized conditions: reaction temperature of 150.0 °C, WFO:methanol molar ratio of 30:1, catalyst amount of 6.0 %, and reaction time of 3.0 h.

The obtained values of ester content in biodiesels using catalysts containing 10.0, 20.0, 30.0, and 40.0 % molybdenum in their final compositions were 44.4 %, 79.4 %, 89.0 %, and 88.8 %, respectively. Accordingly, there is an increase in the ester content of biodiesels as the concentration of molybdenum is high in the catalyst composition. This occurs due to the increase of acidic sites on the surface of the catalysts, since it is at the surface that ion exchange occurs during the reaction process (Gonçalves et al., 2021b; Almeida et al., 2014). In addition, this behavior can be evidenced when comparing the activity of the 10-MoO_3/RHA-$CoFe_2O_4$ and 30-MoO_3/RHA-$CoFe_2O_4$ catalysts which led to the synthesis of biodiesels with ester contents of 44.4 % and 89.0 %, respectively, representing a gain of about 45.0 % of ester content in biodiesel when the catalyst 30-MoO_3/RHA-$CoFe_2O_4$ was employed.

In addition, Fig. 2 shows the determined surface acidity values for the different catalysts studied and highlights a proportional relationship between the increase in the concentration of molybdenum in the final composition of the catalysts and their determined surface acidity values. This can be observed, for example, when comparing the surface acidity values between the 10-MoO_3/RHA-$CoFe_2O_4$ (3.7 mmol H^+ g^{-1}) and 40-MoO_3/RHA-$CoFe_2O_4$ (9.2 mmol H^+ g^{-1}) catalysts, demonstrating a difference in surface acidity of magnitude 5.5 mmol H^+ g^{-1}. In addition,

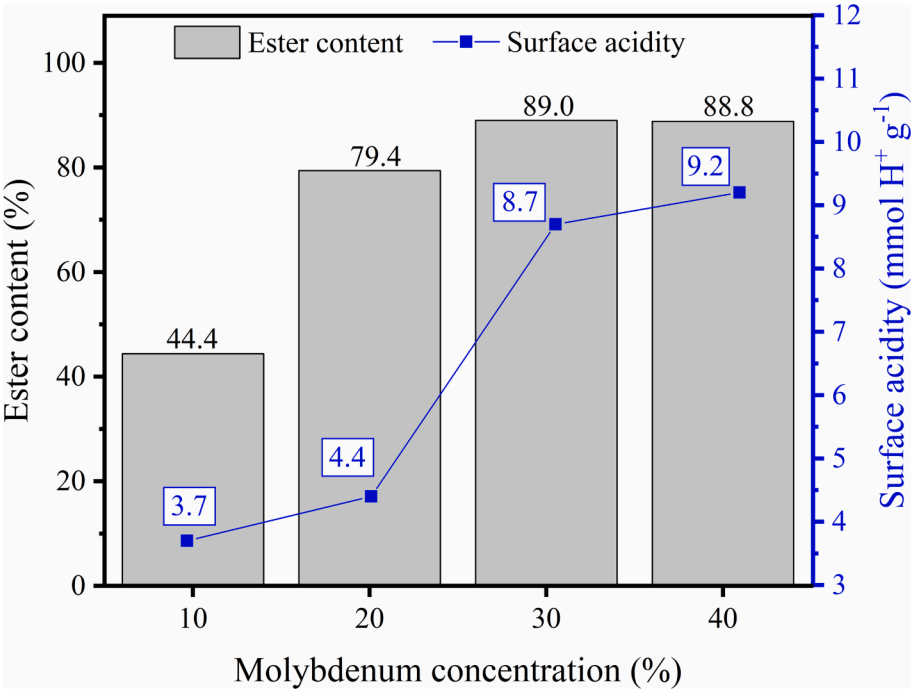

Fig. 2. Influence of molybdenium amount (reaction conditons: reaction temperature of 150 °C, molar ratio methanol:WFO of 30:1, catalyst amount of 6 wt% and reaction time of 3 h).

it is observed that the surface acidity value of the catalyst 30-MoO_3/RHA-$CoFe_2O_4$ (8,7 mmol H^+ g^{-1}) is relatively close to the value of the catalyst 40-MoO_3/RHA-$CoFe_2O_4$, which explains the fact that both catalysts lead to biodiesels with ester contents similar to 89.0 %. In addition, it should be noted that the surface acidity determined for the RHA support was 0.9 mmol H^+ g^{-1} and for $CoFe_2O_4$ was 1.2 mmol H^+ g^{-1}. These values are considerably lower compared to those recorded for the studied catalysts, since the increase of the surface acidity in the catalysts is related to the Brønsted acid sites of MoO_3 impregnated in them (Pinto et al., 2019). Thus, the 30-MoO_3/RHA-$CoFe_2O_4$ catalyst was selected as the most promising for the development of this study due to its high catalytic performance in the biodiesel production process studied preliminarily.

3.2. Catalyst characterization of the catalyst 30-MoO_3/RHA-$CoFe_2O_4$

The X-ray diffractograms referring to MoO_3, $CoFe_2O_4$, RHA, and 30-MoO_3/RHA-$CoFe_2O_4$ are shown in Fig. 3. The diffractogram referring to MoO_3 (in green) shows the presence of peaks related to hexagonal (h-MoO_3) and orthorhombic (α-MoO_3) polymorphic structures from MoO_3. The peaks referring to the hexagonal structure are present in 36.4°, 41.4°, 46.6°, 61.9°, and 62.6°, while the peaks referring to the orthorhombic structure are present in 33.4°, 38.4°, 45.8°, 48.8°, 53.3°, 66.4°, 73.9°, and 78.5° (Pinto et al., 2019; Thangasamy et al., 2018).

The diffractogram concerning $CoFe_2O_4$ (in blue) showed the presence of peaks in 29.1°, 43.2°, 49.2°, 50.2°, 59.0,° and 60.3°, which confirms the spinel structure with cubic face of centered face of ferrite $CoFe_2O_4$ (Racik et al., 2022). In the diffractogram referring to the RHA support (in red), the predominance of the amorphous diffraction pattern is perceived, which is characteristic of amorphous silica, an abundant element in the composition of RHA (Conceição et al., 2017; Caliman et al., 2010). The diffractogram relative to the catalyst 30-MoO_3/RHA-$CoFe_2O_4$ (in black) shows the occurrence of peaks characteristic of both MoO_3 (33.2°, 36.2°, 38.3°, 46.5°, and 66.2°) and of $CoFe_2O_4$ (53.1° and 61.7°), which indicates the presence of these materials in the composition of the catalyst. In addition, it is assumed that the low intensity of the MoO_3 and $CoFe_2O_4$ peaks present in the catalyst can be explained by the high dispersion of the materials in the catalytic support.

The FTIR spectra of the MoO_3, $CoFe_2O_4$, RHA, and 30-MoO_3/RHA-$CoFe_2O_4$ materials are shown in Fig. 4. In the MoO_3-related FTIR spectrum (in green), there is the presence of bands at 806, 837, and 974 cm^{-1}, characteristics of Mo—o and O—Mo—O stretch bond vibrations (Ma et al., 2020). In the FTIR spectrum related to $CoFe_2O_4$ (in blue), there is the presence of the band at 613 cm^{-1}, suggesting the occurrence of Fe(Co)—O bonds in the octahedral and tetrahedral sites, characteristic of the spinel phase of ferrite (Asadi et al., 2022; Kumar et al., 2014). The FTIR spectrum referring to the RHA support (in red) shows the presence of bands at 445, 792, and 1074 cm^{-1}, characteristic of the Si—O—Si symmetric and asymmetric stretch bond vibration of the silica present in RHA (Atta et al., 2012; Helmiyati and Suci, 2019; Parrillo et al., 2021).

In the FTIR spectrum for the 30-MoO_3/RHA-$CoFe_2O_4$ catalyst (in black), the vibrational bands identified at 445, 792, and 1074 cm^{-1} are characteristic of the presence of silica, while the vibrational band at 613 cm^{-1} is related to the spinel phase of ferrite. However, it is possible to observe, in a well attenuated way, the bands at 837 and 974 cm^{-1} concerning the normal vibration modes of the Mo–O bonds present in MoO_3. This low intensity of the MoO_3 peaks present in the catalyst can be explained by the high dispersion of the active phase in the catalytic support, behavior previously observed in a similar way in the XRD analysis.

The morphologies of the MoO_3, $CoFe_2O_4$, RHA, and 30-MoO_3/RHA-$CoFe_2O_4$ materials are shown in Fig. 5. Fig. 5(a), (b), and (c) illustrate the micrographs referring to the MoO_3 magnifications of 5.0 kx, 10.0 kx,

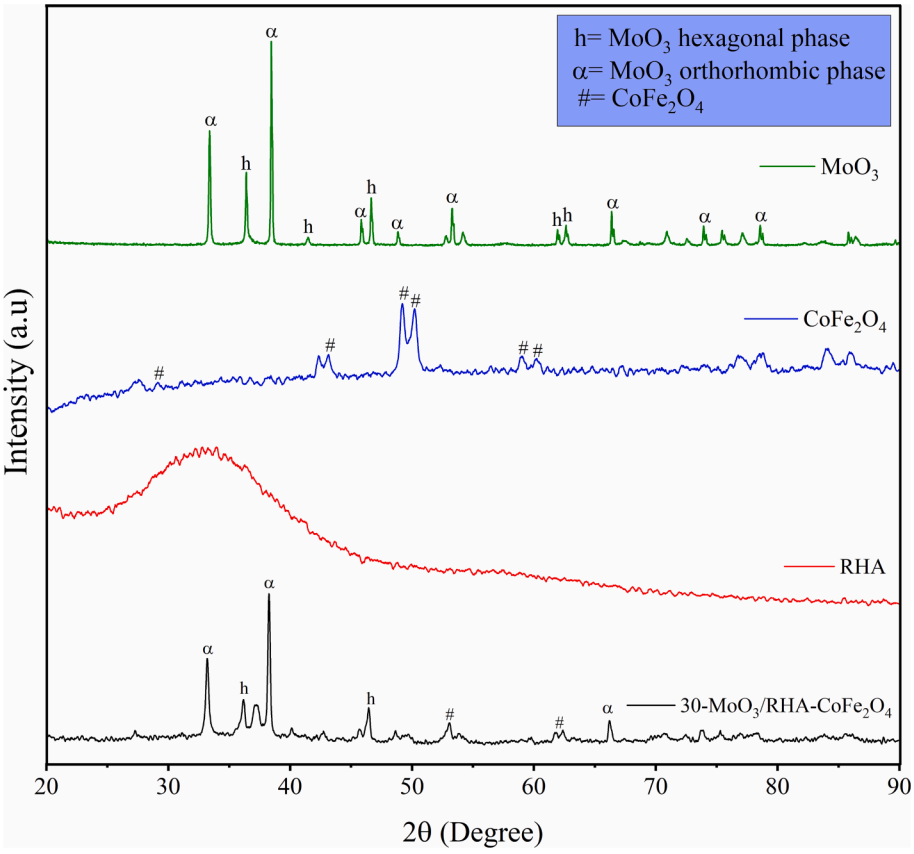

Fig. 3. XDR patterns of MoO_3, $CoFe_2O_4$, RHA and catalyst 30-MoO_3/RHA-$CoFe_2O_4$.

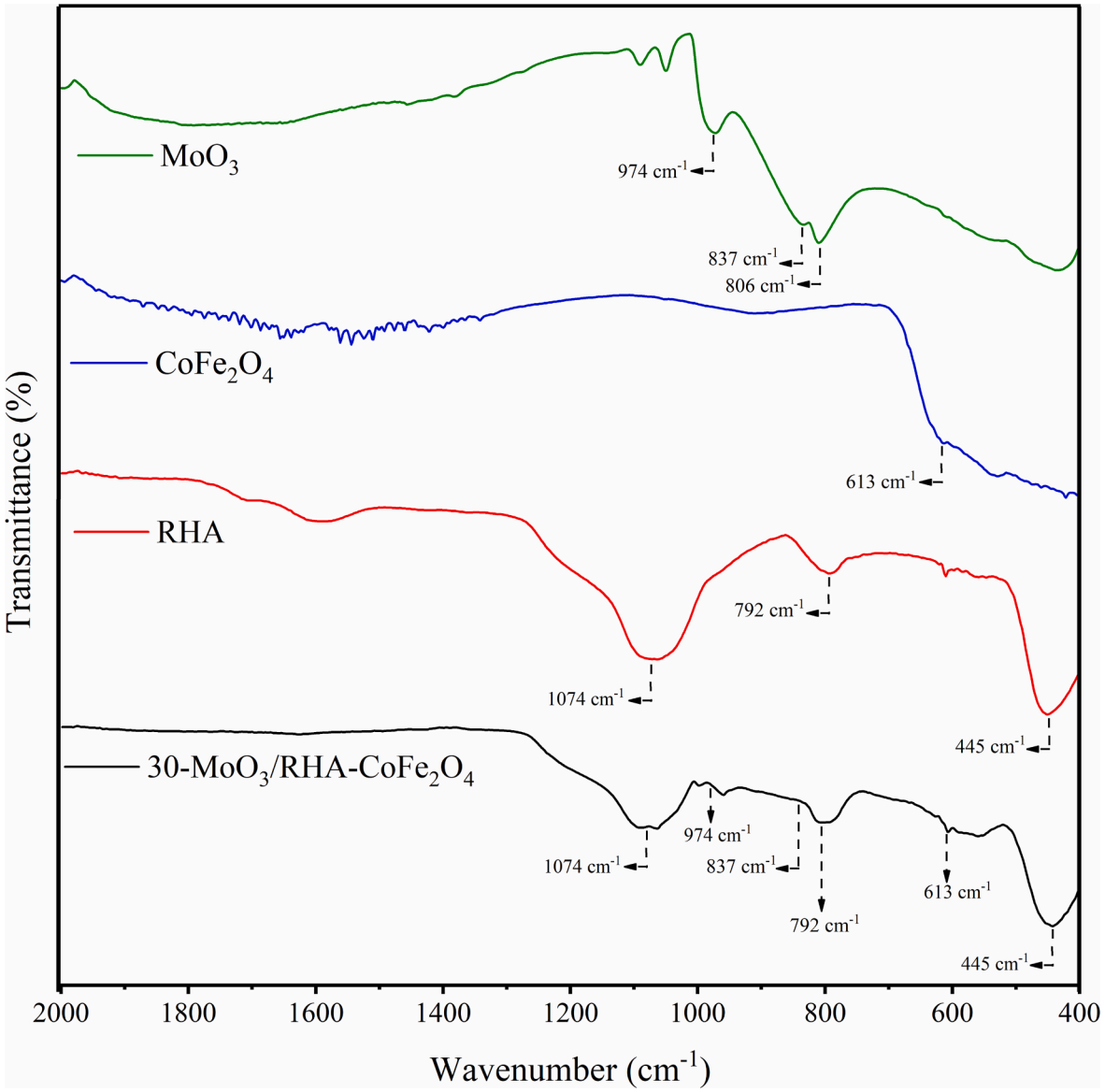

Fig. 4. FTIR spectra of MoO_3, $CoFe_2O_4$, RHA and catalyst 30-MoO_3/RHA-$CoFe_2O_4$.

and 15.0 kx, respectively, and suggest that this material is formed by a cluster of rods with morphologies characteristic of orthorhombic structures of MoO_3, since this structure is predominant in MoO_3 synthesized at temperatures above 400.0 °C (Dhage et al., 2009), as in this study. In Fig. 5(d), (e) and (f), the micrographs referring to the RHA support are shown at magnifications of 200.0x, 1.0 kx, and 2.0 kx, respectively, and suggest the existence of a typical silica-cellulosic structure referring to the external epidermis, such as a corn cob. In addition, it is noteworthy that, in this study, RHA was used without prior treatment and the remaining organic material is due to incomplete pyrolysis of rice husk that generated the RHA (Parrillo et al., 2021; Liu et al., 2014). Fig. 5(g), (h), and (i) shows the micrographs referring to $CoFe_2O_4$ at magnifications of 5.0 kx, 10.0 kx, and 15.0 kx, respectively, and highlights the absence of a defined morphology, as reported by Jayalakshmi & Jeyanthi (2018). Fig. 5(j), (k), and (l) refers to the micrographs of the 30-MoO_3/RHA-$CoFe_2O_4$ catalyst at magnifications of 5.0 kx, 10.0 kx, and 15.0 kx, respectively, and indicates the presence of rods relative to the MoO_3 structures covering the catalyst surface, evidencing the efficiency of the impregnation process adopted in the study.

Fig. 6 shows the composition and elemental maps of the components present in the $CoFe_2O_4$ support and the 30-MoO_3/RHA-$CoFe_2O_4$ catalyst. From the $CoFe_2O_4$ EDS spectrum, show in Fig. 6(a), the existence of the elements Fe (25.12 wt%), Co (51.56 wt%) and O (23.31 wt%) in the $CoFe_2O_4$ structure surface is confirmed. The peaks located at approximately 0.5 and 6.5 Kev are related to the absorption energy dissipated by the iron, while the cobalt element shows peaks located at approximately 0.7, 7.0 and 7.6 Kev, which is the majority element because of the higher intensity of the peaks. In addition, it can be seen that oxygen showed only one high-intensity peak at 0.5 Kev, indicating that the components are in the form of oxides. Based on the percentage values of Fe and Co, the Co^{2+} to Fe^{3+} ratio is estimated at 1:2.05, extremely close to the 1:2 ratio (Co^{2+}:Fe^{3+}) used in the $CoFe_2O_4$ synthesis method. The elementary mapping of $CoFe_2O_4$ (Fig. 6(b)) shows a homogeneous and uniform distribution of the elements constituting the magnetic support, indicating the efficiency of the coprecipitation process employed.

Fig. 6(c) shows the spectrum referring to the catalyst composition and indicates the content of 28.23 % molybdenum in its composition, a value close to the desired percentage of 30.0 %, which suggests the success of the impregnation method adopted in the study. In addition, the element with the highest percentage in the catalyst composition is oxygen with a content of 38.28 %. This data is corroborated by the fact

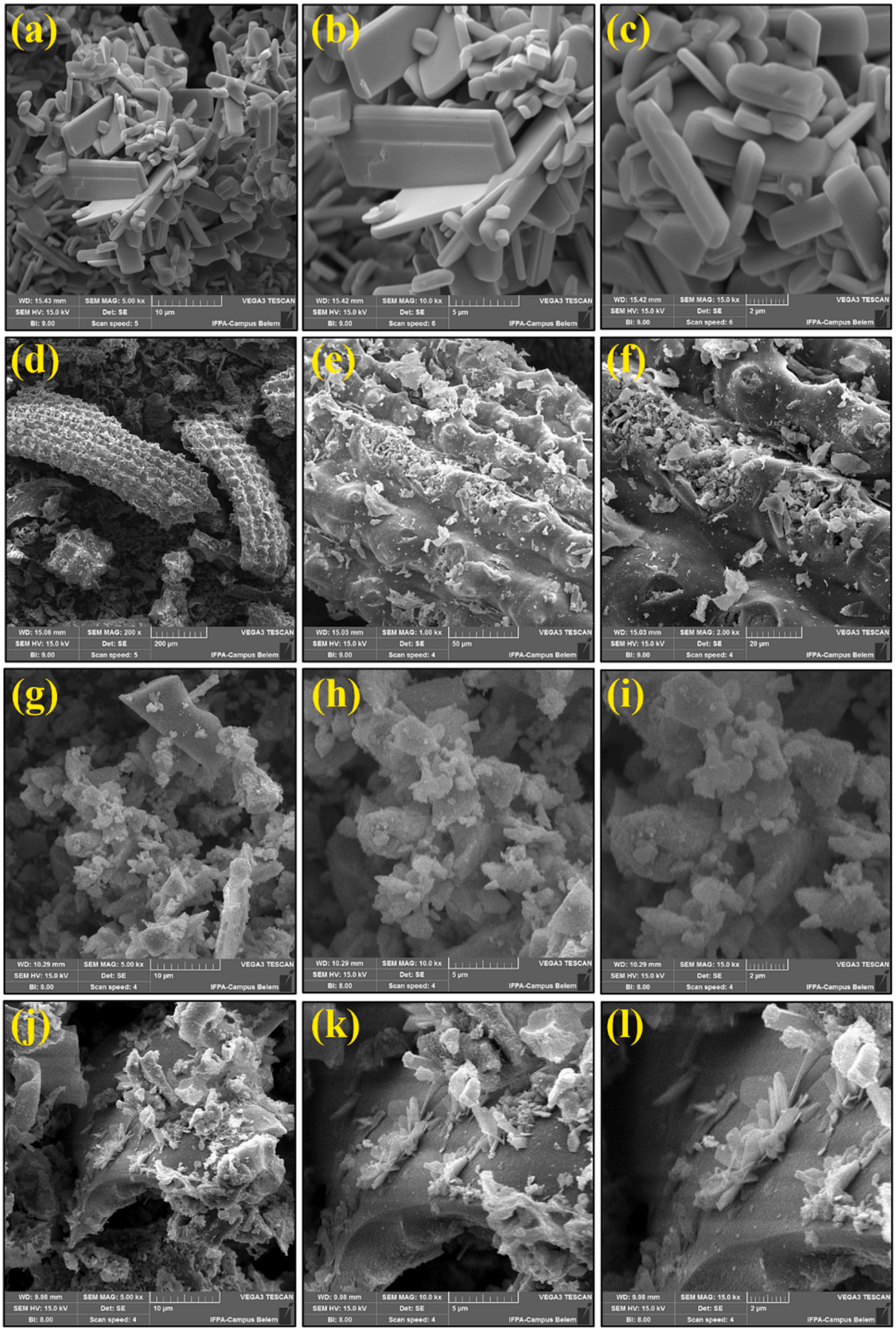

Fig. 5. SEM images of (a) MoO_3 5000x magnification, (b) MoO_3 10000x magnification, (c) MoO_3 15000x magnification, (d) RHA 200x magnification, (e) RHA 1000x magnification, (f) RHA 2000x magnification, (g) $CoFe_2O_4$ 5000x magnification, (h) $CoFe_2O_4$ 10000x magnification and (i) $CoFe_2O_4$ 15000x magnification, (j) 30-MoO_3/RHA-$CoFe_2O_4$ 5000x magnification, (k) 30-MoO_3/RHA-$CoFe_2O_4$ 10000x magnification and (l) 30-MoO_3/RHA-$CoFe_2O_4$ 15000x magnification,

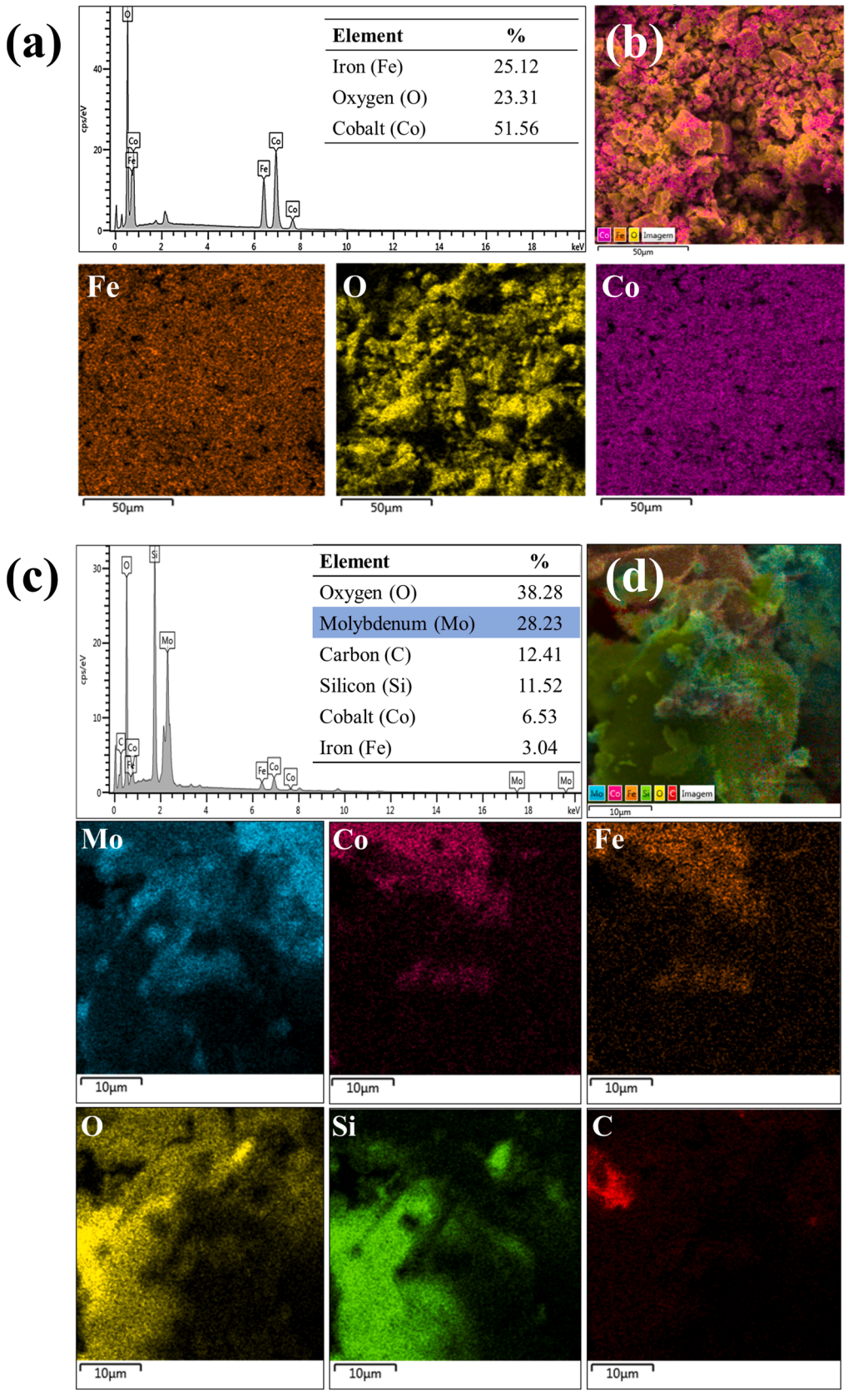

Fig. 6. EDS composition of (a) $CoFe_2O_4$, (b) elemental maps of each component of the $CoFe_2O_4$ (c) catalyst 30-MoO_3/RHA-$CoFe_2O_4$ and (d) elemental maps of each component of the catalyst 30-MoO_3/RHA-$CoFe_2O_4$.

that the catalyst is mostly composed of oxides. The percentages of cobalt (6.53 %) and iron (3.04 %) indicate the success of the desired Fe:Co = 2 ratio in the synthesis step. Finally, the presence of carbon at a content of 12.41 % can be attributed to the presence of C—C and C═O groups, due to the partial thermal decomposition of biomass.

Fig. 6(d) shows the elemental surface mapping of the catalyst as well as the other elemental maps of each component. From the analysis of the maps, it is realized that the elements molybdenum and oxygen are widely dispersed over the entire surface of the 30-MoO_3/RHA-$CoFe_2O_4$ catalyst. In addition, the maps show that the elements iron and cobalt also have wide dispersion and are related to each other in the same regions of the catalyst surface, evidencing the presence of $CoFe_2O_4$ in the composition of the catalyst.

The magnetic properties of $CoFe_2O_4$ and 30-MoO_3/RHA-$CoFe_2O_4$ were studied using the VSM technique, by obtaining M−H hysteresis curves (magnetization-applied (M) vs magnetic field (H)), as shown in Fig. 7. From the analysis of Fig. 7, it is realized the ferromagnetic behavior for $CoFe_2O_4$ and 30-MoO_3/RHA-$CoFe_2O_4$ with their saturation magnetization (Ms) values being 12.7 emu g^{-1} and 7.0 emu g^{-1}, respectively. The decrease in Ms value of $CoFe_2O_4$ in comparison to 30-MoO_3/RHA-$CoFe_2O_4$ Ms value is due to the fact that the catalyst has only 30 % $CoFe_2O_4$ in its composition, in addition to the presence of other elements without magnetic properties, such as RHA and molybdenum. However, the Ms value obtained for the 30-MoO_3/RHA-$CoFe_2O_4$ catalyst is sufficient to promote its separation by applying a magnetic field, as well as is significantly higher in comparison to other catalytic magnetic solids applied to biodiesel production. In the study developed by Tang et al. (2012) the saturation magnetization of the Ca/Al/Fe_3O_4 magnetic catalyst applied to biodiesel production was 6.3 emu g^{-1}. Shi et al. (2017) reported Ms = 4.0 emu g^{-1} for the CaO@ γ-Fe_2O_3 magnetic catalyst used in transesterification reaction. In another study, Wang et al. (2019) reported Ms = 3.7 emu g^{-1} to the ZrFe-SA-SO_3 magnetic catalyst applied in oleic acid esterification for biodiesel synthesis.

3.3. Catalytic performance

The study of optimization of transesterification reaction parameters using the catalyst 30-MoO_3/RHA-$CoFe_2O_4$, such as reaction temperature, methanol:WFO molar ratio, catalyst amount, and reaction time was performed using the OVAT methodology. The results obtained are shown in Fig. 8.

The optimization study of the reaction temperature, shown in Fig. 8 (a), was conducted in the range of 130.0 °C to 170.0 °C, keeping constant the variables methanol:WFO molar ratio, catalyst amount and reaction time in 30:1, 5.0 wt%, and 3.0 h, respectively. From the analysis of the results present in Fig. 8(a), it is possible to notice an increase in the ester content in the biodiesels obtained as the reaction temperature of the process increases, reaching the highest ester content value of 94.7 % for the biodiesel obtained in the reaction performed at 160.0 °C. This occurs due to the increase in temperature in the reaction process providing an increase in collisions of the reactant molecules, leading to an increase in the miscibility of the reaction medium, which in turn favors mass transfer, resulting in an increase in the ester content of the biodiesel produced (Ashok and Kennedy, 2019). However, when the catalyst is used in the reaction at 170.0 °C, the obtained biodiesel has an ester content of 87.5 %, indicating a decrease in ester content when compared to the synthesized biodiesel at 160.0 °C. This suggests a negative effect of the increase in temperature, indicating the reach of the reaction equilibrium in relation to the process temperature (Gardy et al., 2018). In this sense, the value of 160.0 °C was chosen as the optimized value for reaction temperature due to the fact that it provides the highest ester content value to the synthesized biodiesel.

The results of the optimization of the variable methanol:WFO molar ratio are shown in Fig. 8(b). The study was conducted in the range of

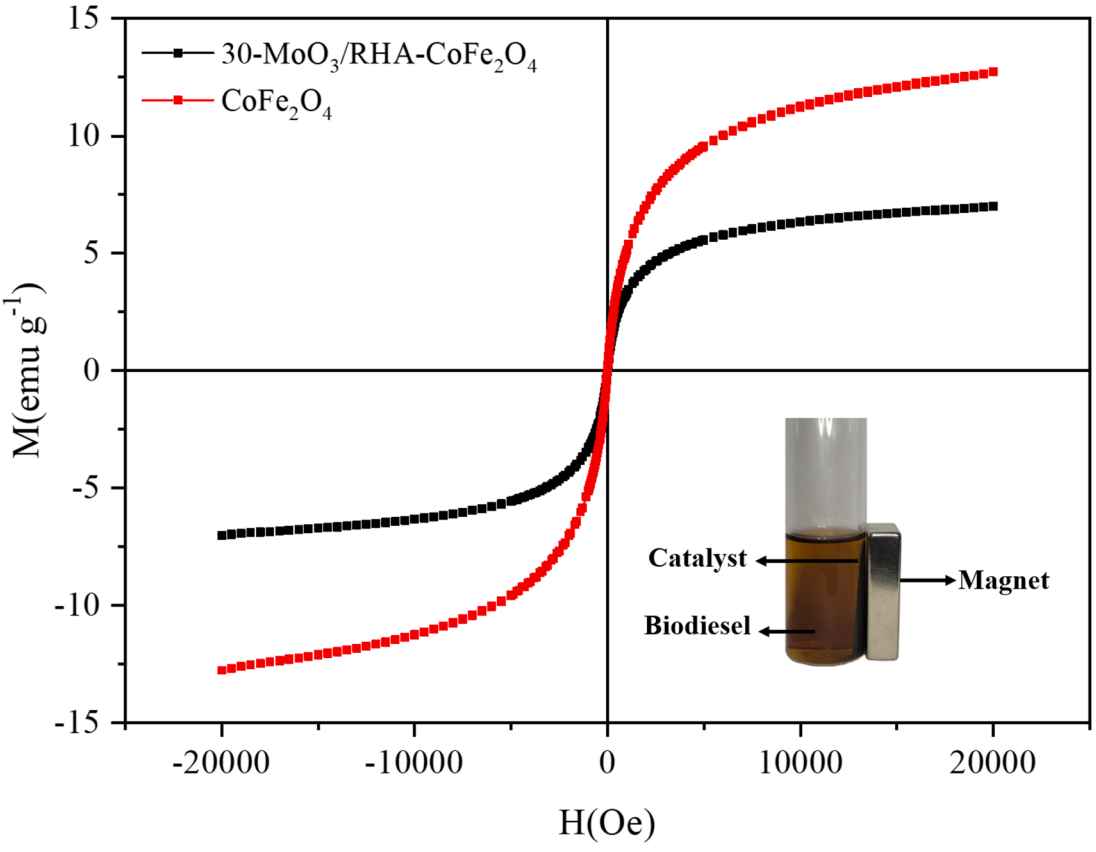

Fig. 7. VSM characterization for$CoFe_2O_4$ and 30-MoO_3/RHA-$CoFe_2O_4$.

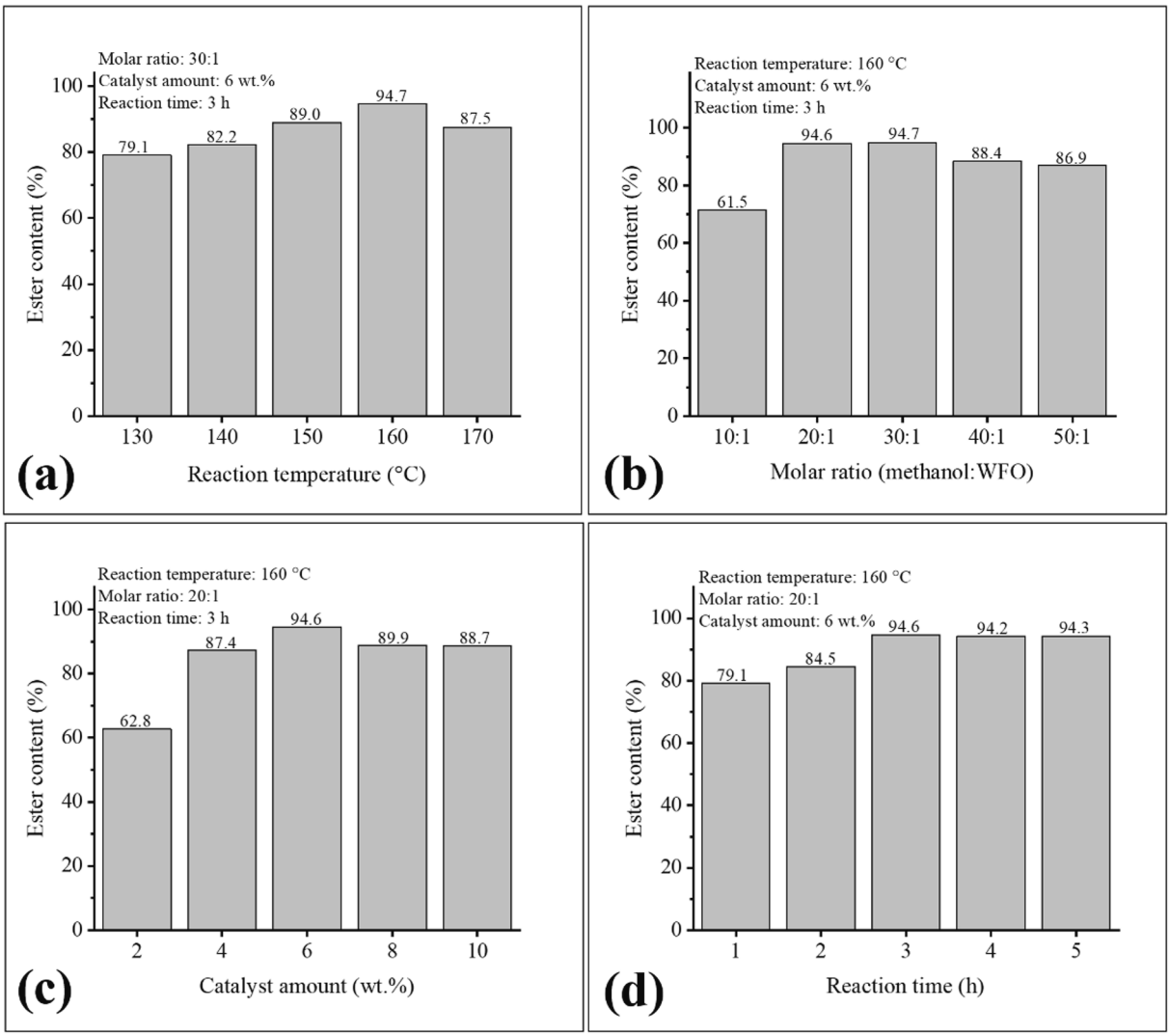

Fig. 8. Effect of (a) reaction temperature, (b) molar ratio methanol:WFO, (c) catalyst amount and (d) reaction time on ester content.

10:1 to 50:1, keeping constant the variables reaction temperature, catalyst amount, and reaction time at 160.0 °C, 6.0 wt%, and 3.0 h, respectively. The analysis of the results show that, initially, when processing the reactions by raising the methanol:WFO molar ratio values, biodiesels with high ester contents are obtained, for example biodiesel with ester content of 61.5 % obtained using the methanol:WFO molar ratio of 10:1, while the reaction using the methanol:WFO molar ratio of 30: 1 provided a biodiesel with ester content of 94.7 %. This behavior may be related to the excess of methanol used, leading to greater miscibility of the reaction medium, which in turn leads to an increase in the number of collisions between the reactant molecules (Foroutan et al., 2022; Pinto et al., 2019). However, it is observed that the use of methanol:WFO molar ratio above 30:1 in the reaction process leads to a decrease in the ester content values of biodiesels, such as those obtained using the molar ratios of 40:1 (88.4 %) and 50:1 (86.9 %). This is due to the fact that the high excess of methanol used causes saturation of the catalytic surface at a certain point, causing deactivation of the catalyst, decreasing the efficiency of the transesterification reaction (Aziz et al., 2017). In this sense, the methanol:WFO molar ratio of 20:1 was selected because the synthesized biodiesel reached an ester content of 94.6 %, a value relatively similar to biodiesel produced using the molar ratio of 30:1 (94.7 %).

The catalyst amount optimization study, shown in Fig. 8(c), was conducted in the range of 2.0 to 10.0 wt%, keeping the other variables at 160.0 °C, methanol:WFO molar ratio of 20:1, and reaction time of 3.0 h. The results show an increase in the ester content values of the synthesized biodiesels as there is an increase in the amounts of the catalysts used in the values of 2.0 wt% to 6.0 wt%. This is due to the greater amount of active sites in the reaction medium as the amount of catalyst used in the reaction increases (Mohebbi et al., 2020; Olubunmi et al., 2022). However, when catalyst amounts above 6.0 wt% are used in the reaction, there is a decrease in the ester content values of biodiesels, such as 89.9 % and 88.7 %, for catalyst amounts of 8.0 wt% and 10.0 wt %, respectively. This behavior is due to the fact that the increase in the amount of catalyst used causes limitations in mass transfer that reduces the interaction of active sites with the reactants. It can also cause problems related to catalyst diffusion in the reaction medium (Zhang et al., 2022; Olubunmi et al., 2022). Thus, the optimized value of the catalyst amount variable chosen was 6.0 wt%.

The optimization study for the reaction time variable is shown in Fig. 6(d) and was conducted in the range of 1.0 to 5.0 h, under conditions of reaction temperature of 160.0 °C, methanol:WFO molar ratio of 20:1, and catalyst amount of 6.0 wt%. The exposed results show an increase in the ester content values of the biodiesels produced as there is an increase in the reaction time. This can be visualized considering the use of reaction times of 1.0 and 3.0 h, which led to biodiesels with ester contents of 79.1 % and 94.6 %, respectively. However, reactions using reaction times from 3.0 h up do not provide an increase in ester contents

in biodiesels, as can be seen in biodiesels obtained using reaction times of 4.0 and 5.0 h that led to ester contents of 94.2 % and 94.3 %, respectively. This slight decrease is probably due to the reversible nature of the transesterification reaction after reaching equilibrium (Santos et al., 2022). In this sense, the reaction time selected in the optimization of this study was 3.0 h, since it provides the highest ester content among the biodiesels studied.

3.4. Biodiesel characterization

Biodiesel produced using 30-MoO_3/RHA-$CoFe_2O_4$ catalyst in the optimized conditions of the transesterification reaction was evaluated in order to determine the quality of its physicochemical properties, as shown in Table 2. From the results presented, it can be observed that the kinematic viscosity parameter obtained a value of 4.33 $mm^2\ s^{-1}$, while the density showed a value of 0.887 g cm^{-3}. These values comprise the limits stipulated by the ASTM D6751 and EN 14214 standards and contribute fundamentally to the evaluation of biodiesel quality, since they are directly related to the fuel injection system in the engine and to problems related to impurity deposits throughout the vehicle engine (Mares et al., 2021; Mawlid et al., 2022).

The value determined for the flash point property of biodiesel was 155.0 °C. This high value represents a very important parameter in terms of safety because biodiesel can be handled, stored, and transported in ambient conditions without offering risks. The determined copper corrosivity parameter of biodiesel was 1a, which means absence of corrosion according to the ASTM Copper Strip Corrosion Standard Classification. This, together with the fact that this value complies with the ASTM D6751 and EN 14214 standards, corroborates the high quality of the synthesized biodiesel. In addition, the cold filter clogging point for biodiesel was 0.0 °C, suggesting good applicability of this biofuel even in cold climate regions (Santos et al., 2022). Another important property determined was the acidity index, for which the biodiesel obtained a value of 0.24 mg KOH g^{-1}. The monitoring of this property in biodiesel is of fundamental importance, especially during its storage, since changes in the values in this step can mean the presence of water in the biodiesel, which can trigger the formation of acids, promoting the biodiesel oxidation process (Santos et al., 2022). Thus, all the results obtained in the characterization of biodiesel proved to be adequate to international standards, suggesting that the biofuel produced will not cause problems in the engine, such as corrosion, impurity deposits, thermal instability, and problems related to its use at low temperatures (Mares et al., 2021; Mawlid et al., 2022).

The gas chromatography technique was employed in order to evaluate the ester content of biodiesel produced in this study. In this sense, the composition in methyl esters of biodiesel produced from WFO were obtained, as shown in Fig. 9. Through the analysis of the chromatogram present in Fig. 9(a), the presence of six peaks is perceived, five of which are related to the esters that make up biodiesel (1, 3, 4, 5, and 6) and one

Table 2
Physicochemical properties of the biodiesel produced at optimized conditions.

Properties	Test methods	Limits		This study
		ASTM D 6751	EN 14,214	
Kinematic viscosity, at 40 °C ($mm^2\ s^{-1}$)	ASTM D445	1.9–6.0	3.5–5.0	4.33
Density, at 15 °C (g cm^{-3})	ASTM D1298	–	0.86–0.90	0.887
Flash point (°C)	ASTM D93	>130.0	>120.0	155.0
Copper strip corrosion	ASTM D130	<3.0	1	1a
Cold filter plugging point (°C)	ASTM D6371	NS	–	0.0
Acid value (mg KOH g^{-1})	ASTM D664	<0.8	<0.5	0.24

NS = Not specified.

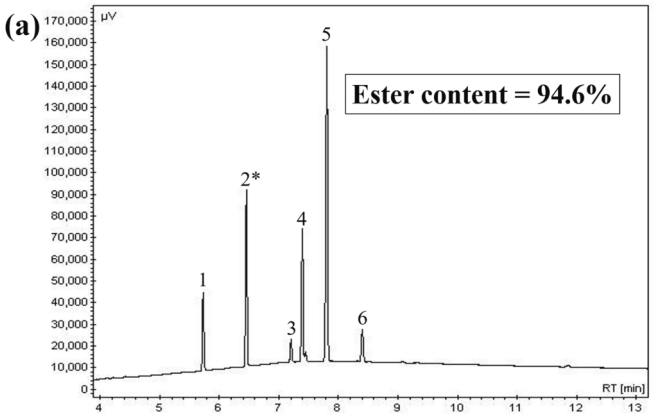

(b)

Peak	Fatty acid of methyl ester	Retention time (min)	Area (%)
1	Methyl palmitate ($C_{17}H_{34}O_2$)	5.73	9.26
2*	Methyl heptadecanoate ($C_{18}H_{36}O_2$)	6,46	20.07
3	Methyl stearate ($C_{19}H_{38}O_2$)	7.21	2.81
4	Methyl oleate ($C_{19}H_{36}O_2$)	7.40	18.23
5	Methyl linoleate ($C_{19}H_{34}O_2$)	7.81	44.37
6	Methyl linolenate ($C_{19}H_{32}O_2$)	8.40	5.25
* Internal standard			

Fig. 9. (a) GC chromatogram and (b) composition for biodiesel produced using the catalyst 30-MoO_3/RHA-$CoFe_2O_4$.

is related to the internal standard used methyl heptadecanoate (2*). In addition, through the analysis of Fig. 9(b), the predominance of methyl linoleate (44.37 %) and methyl oleate (18.23 %) esters is perceived, which is an expected fact, since they are derivatives of their respective fatty acids, linoleic and oleic, mostly present in the composition of soybean oil (Zhang et al., 2022; Gonçalves et al., 2021b).

3.5. Evaluation of the recyclability

After the optimization of the transesterification reaction variables, the stability of the catalytic property of the catalyst was investigated when employing it in several reaction cycles. Fig. 10 shows the reusability study of the 30-MoO_3/RHA-$CoFe_2O_4$ catalyst performed under the following optimized conditions: 160.0 °C reaction temperature, methanol:WFO molar ratio of 20: 1, catalyst amount of 6.0 wt%, and

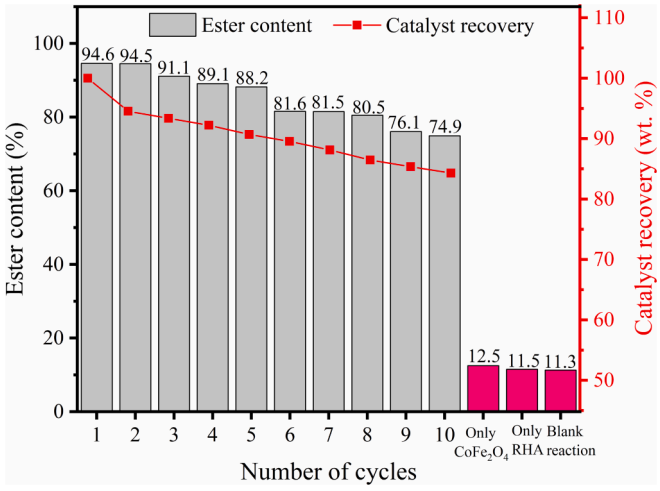

Fig. 10. Reusability and recovery of the catalyst 30-MoO_3/RHA-$CoFe_2O_4$.

reaction time of 3.0 h.

From the analysis of Fig. 10, it is possible to obtain 94.6 % ester content for the biodiesel produced in the first reaction cycle and the maintenance of ester content in biodiesels above 70.0 % over 10 reaction cycles, which indicates the high catalytic stability of the catalyst studied. In addition, it is worth mentioning that the ester content value obtained for the synthesized biodiesel in the tenth reaction cycle (72.1 %) was considerably higher than the ester content of biodiesels obtained in the reactions performed using only $CoFe_2O_4$ (12.5 %), the RHA support (11.5 %), and without the presence of the catalyst (blank reaction) (11.3 %), thus indicating the catalytic robustness of the catalyst 30-MoO_3/RHA-$CoFe_2O_4$ in relation to other solid acid catalysts reported in the literature. It is also worth noting the catalyst recovery efficiency through magnetism, as shown in Fig. 10.

However, despite the high catalytic stability of the catalyst 30-MoO_3/ RHA-$CoFe_2O_4$, the determining factor for the decrease of ester contents in biodiesels (approximately 20.0 %) over the ten reaction cycles was studied. For this, EDS analysis was performed for the catalyst recovered after the tenth reaction cycle in order to determine its elemental composition, as shown in Fig. 11(a). The analysis of this data shows that there was an increase in the carbon content present (20.11 %) when compared to the carbon content of 12.41 % initially determined in the catalyst 30-MoO_3/RHA-$CoFe_2O_4$ (Fig. 6). This may be related to the probable deposit of organic materials on the surface of the catalyst, residues from unconverted reagents, products and co-products, which cause obstruction of the active sites, directly compromising the catalytic activity (Santos et al., 2022). In addition, the decrease in the molybdenum content present in the catalyst should be noted. It was initially 28.23 % and went to a content of 19.48 % in the catalyst after the tenth reaction cycle. This is probably due to the phenomenon of leaching, which is also corroborated by the decrease in the acidity of the catalyst surface of 8.7 mmol^{+} g^{-1} to 4.1 mmol H^{+} g^{-1} (Oliveira et al., 2019).

The magnetic property of the catalyst throughout the reaction cycles was also evaluated, as shown in Fig. 11(b). Through the analysis of Fig. 11(b), a slight decrease in the value of catalyst saturation magnetization is identified after the tenth cycle, but without significant effect since it was possible to easily separate the catalyst by applying a magnetic field.

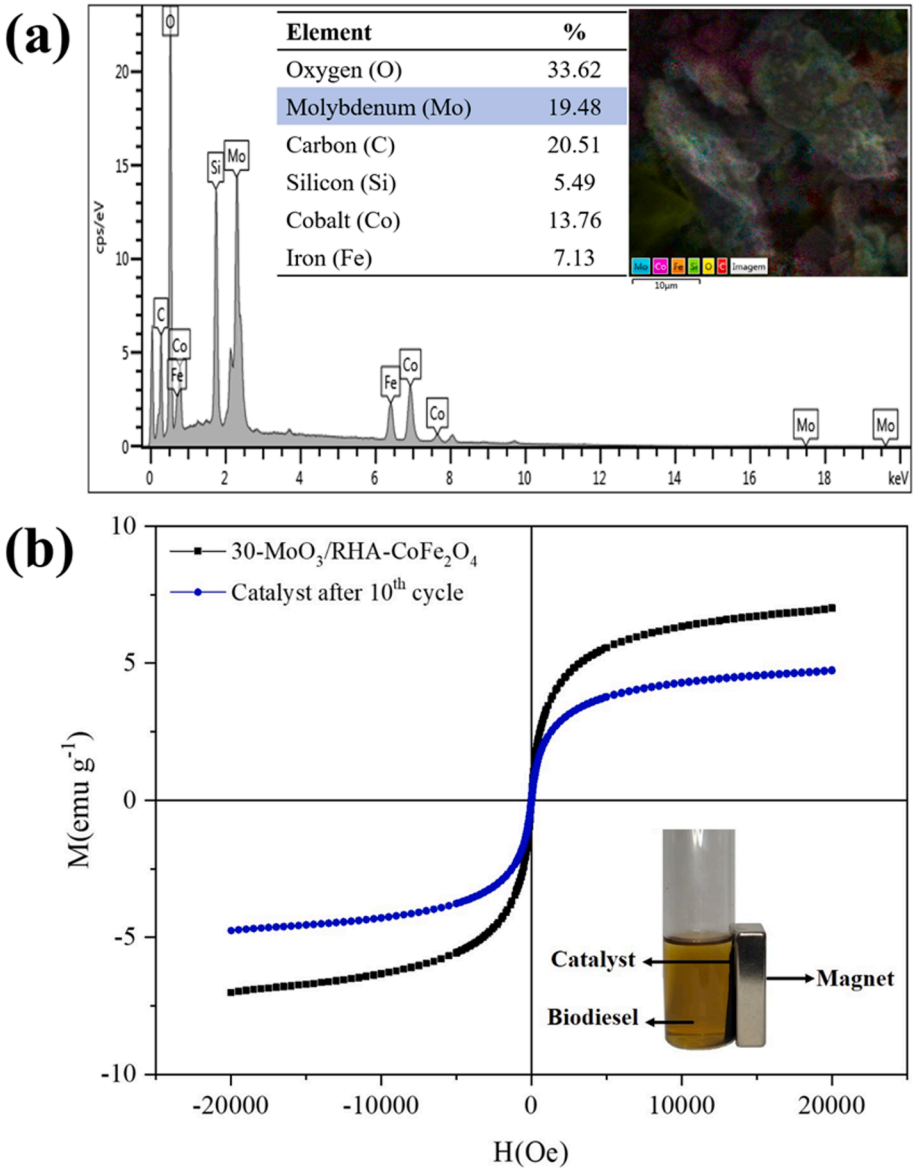

Fig. 11. EDS composition of (a) recovered catalyst 30-MoO_3/RHA-$CoFe_2O_4$ and (b) VSM characterization for the recovered catalyst 30-MoO_3/RHA-$CoFe_2O_4$.

3.6. Kinetic study

The kinetic study, shown in Fig. 12, for the WFO transesterification process using the catalyst 30-MoO_3/RHA-$CoFe_2O_4$ was performed under optimized reaction conditions at four different temperatures: 130.0 °C, 140.0 °C, 150.0 °C, and 160.0 °C. The reaction behavior was assumed to be of (pseudo) first order due to the excess of alcohol used (Mawlid et al., 2022; Kaur et al., 2018). Thus, the pseudo-first reaction is expressed in Eq. (2), below.

$$-\ln(1-x) = kt \tag{2}$$

where 'x 'is the ester content obtained at time't'.

For the values of the 'k' rate constants due to temperature, transesterification reactions were performed at temperatures 130.0 °C, 140.0 °C, 150.0 °C, and 160.0 °C, as shown in Fig. 12 (a). From the analysis of Fig. 12(a), a linear behavior is perceived, typical of a (pseudo) first order reaction. The activation energy (Ea) for the transesterification of WFO with methanol was estimated by Eq. (3), below.

$$lnk = -\mathrm{Ea}/\mathrm{RT} + \mathrm{lnA} \tag{3}$$

where R is the constant of the gases (8.31 J K^{-1} mol^{-1}) and T is the temperance in Kelvin.

The Ea value determined was 27.3 kJ mol^{-1}, from the analysis of the plot 'ln k' vs' 1 / T', as shown in Fig. 12(b). Ea values above 25.0 kJ mol^{-1} indicate that the reaction is chemically controlled and has no diffusion and mass transfer limitations (Mawlid et al., 2022; Kaur et al., 2018).

The thermodynamic parameters determined for the transesterification ration were enthalpy ($\Delta H^{\#}$), entropy ($\Delta S^{\#}$) and Gibbs free energy ($\Delta G^{\#}$). Enthalpy and entropy were calculated using the Eyring-Polanyi Eq. (4) and the plot referring to 'ln (k/T)' *versus* '1/T', as shown in Fig. 12(c).

$$\ln\left(\frac{K}{T}\right) = -\frac{\Delta H^{\#}}{\mathrm{RT}} + \ln\left(\frac{k_B}{h}\right) + \frac{\Delta S^{\#}}{R} \tag{4}$$

where K_B and h are the Boltzmann (1.38 × 10^{-23} J K^{-1}) and Planck (6.63 x 10^{-34} J s) constants, respectively.

In addition, the value of $\Delta G^{\#}$ was determined by Eq. (5), below.

$$\Delta G^{\#} = \Delta H^{\#} - T\Delta S^{\#} \tag{5}$$

All values of the thermodynamic parameters are shown in Table 3. The values obtained for $\Delta H^{\#}$, $\Delta S^{\#}$, and $\Delta G^{\#}$, for different temperatures, were 23.83 kJ mol^{-1}; −0,23 kJ mol^{-1} K^{-1}; 116.4 kJ mol^{-1}; 118.7 kJ mol^{-1}; 120.9 kJ mol^{-1}; and 123,2 kJ/mol.

The positive value of $\Delta H^{\#}$ indicates that for the formation of the transition state energy supply is necessary, characterizing the endothermic nature of the reaction carried out (Mawlid et al., 2022). The negative value of $\Delta S^{\#}$ indicates a higher ordering in the transition state when compared to the reactants (Kaur et al., 2018; Beall, 1994). In addition, the positive value of $\Delta G^{\#}$ indicates the non-spontaneity and endorgonic nature of the transesterification reaction carried out (Kaur et al., 2018; Beall, 1994).

Table 3
Thermodynamic parameters regarding the reaction of WFO into biodiesel using 30- MoO_3/RHA-$CoFe_2O_4$ catalyst.

$\Delta H^{\#}$ (KJ mol^{-1})	$\Delta S^{\#}$ (KJ mol^{-1} K^{-1})	$\Delta G^{\#}$ (KJ mol^{-1})			
		403 K	413 K	423 K	433 K
23.83	–0.23	116.4	118.7	120.9	123.2

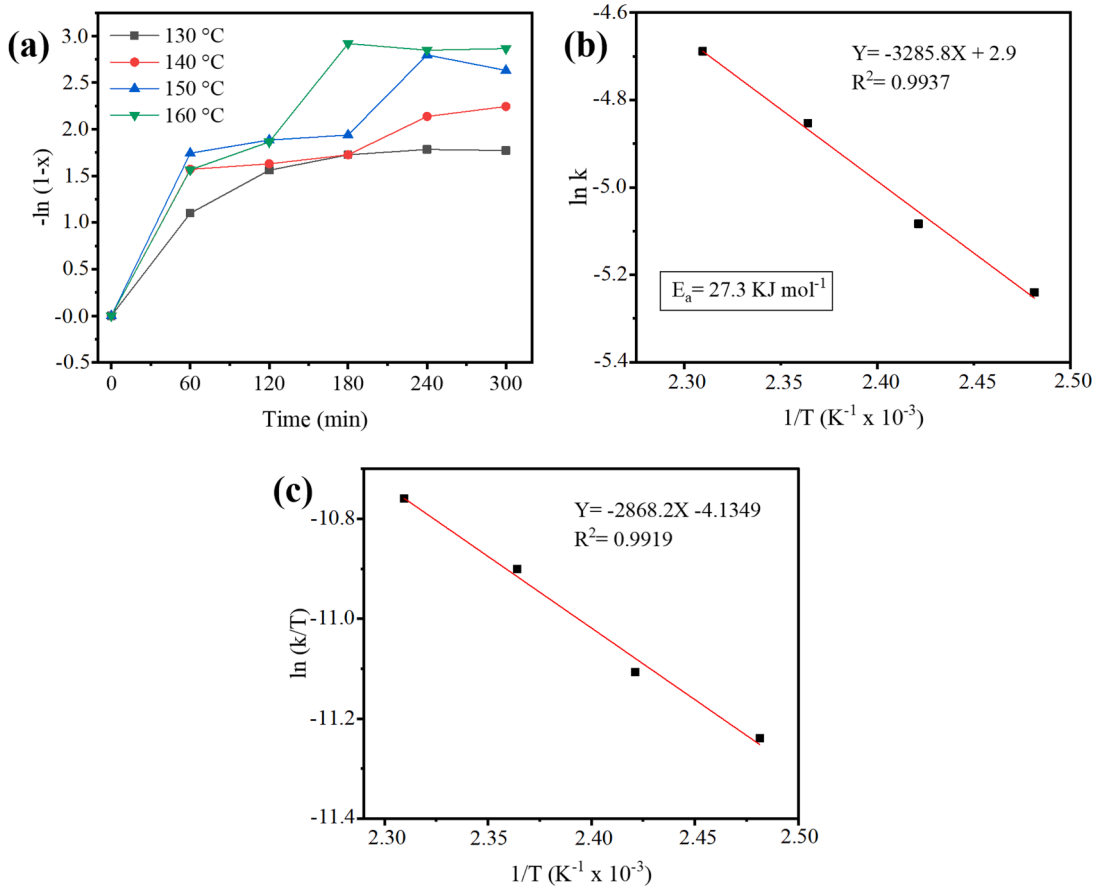

Fig. 12. Plot of (a) -ln(1-X) *versus* reaction time (t) at different temperatures, (b) Arrhenius for activation energy determination and (c) ln (K/T) *versus* 1/T.

3.7. Transesterification reaction and proposed mechanism using the 30-MoO_3/RHA-$CoFe_2O_4$ catalyst

The transesterification reaction is depicted by the overall reaction presented in Fig. 13(a). This process consists of three distinct and reversible phases that occur sequentially. The initial phase involves the conversion to monoacylglicerols, followed by the subsequent phase, which encompasses the transformation of monoacylglicerols into glycerol (Zhang et al., 2022; Adhikesavan et al., 2022). The proposed reaction mechanism for the action of the 30-MoO_3/RHA-$CoFe_2O_4$ catalyst in the transesterification process occurs essentially through a sequence of three steps (Zhang et al., 2022), as shown in Fig. 13(b). Firstly, triacylglycerol molecules are adsorbed onto the catalyst's surface, allowing for a greater interaction between the electron pair of the carbonyl oxygen and the Brønsted and Lewis acid sites present in the catalyst's structure, resulting in an increase in positive charge density on the carbon of the carbonyl (Step 1). This leads to the formation of a carbocation that undergoes a nucleophilic attack from the electron pair of the hydroxyl group in the methanol molecule, forming a tetrahedral intermediate (Step 2). Finally, the tetrahedral intermediate eliminates a molecule of methyl ester and generates a diacylglycerol molecule, along with the regeneration of the acid site of the catalyst (Step 3). This process occurs when the methyl ester is desorbed from its surface, making the catalyst's surface available for the next catalytic cycles. Through processes similar to this, monoacylglycerol and glycerol are formed.

3.8. Comparative study of heterogeneous acids catalysts for biodiesel production

Table 4 shows the comparison of the 30-MoO_3/RHA-$CoFe_2O_4$ catalyst with other solid acid catalysts applied to biodiesel production reported in the literature. Through the analysis of Table 4, it can be seen that the optimized condition obtained for the present study (160.0 °C reaction temperature, methanol:WFO molar ratio of 20:1, catalyst amount of 6.0 wt%, and reaction time of 3.0 h) presents lower values than reported at temperature, but with similar catalytic performance,

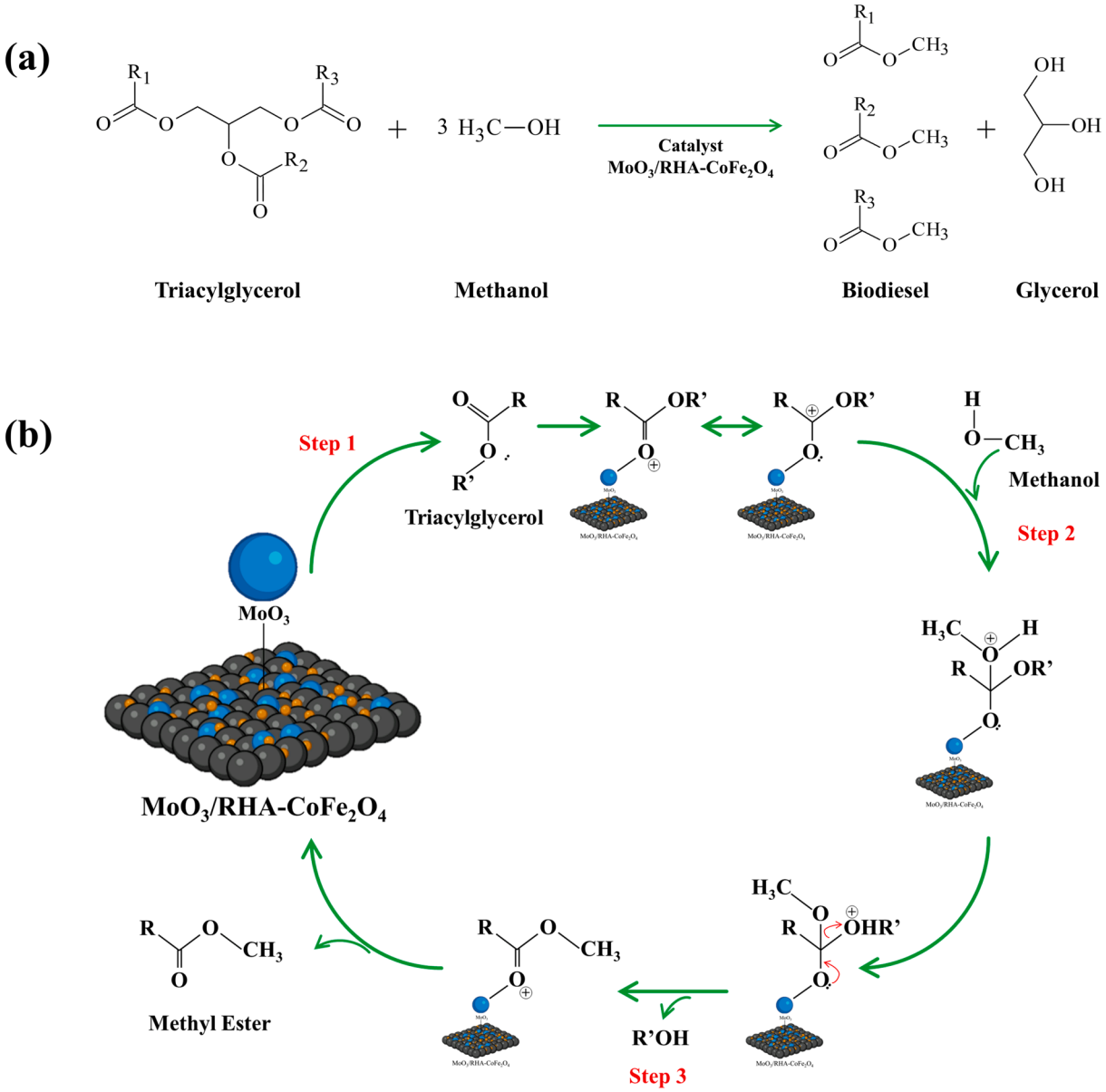

Fig. 13. (a) Transesterification reaction and (b) proposed mechanism using the 30-MoO_3/RHA-$CoFe_2O_4$ catalyst.

Table 4
Comparison of the 30-MoO_3/RHA-$CoFe_2O_4$ catalyst with other solid acid catalysts reported in the literature.

Catalyst	Oil Feedstocks	Reaction conditions				Ester content (%)	Cycles	Reference
		T (°C)	Molar ratio	Catalyst amount (%)	t (h)			
$HPMo/Nb_2O_5$	Macaw	210.0	90:1	20.0	4.0	99.65	4	Conceição et al., 2017
$HPMo/TiO_2$	WCO	190.0	90:1	5.0	4.0	94.5	4	Gonçalves et al., 2021a
25 %MoO_3/ZSM-5	Oleic acid	160.0	20:1	3.0	6.0	98.0	6	Mohebbi et al., 2020
5Mo/ZSM-22	WCO	140.0	9:1	2.0	12.0	78.2	4	Zhang et al., 2022
$MoO_3/SrFe_2O_4$	WCO	164.0	40:1	10.0	4.0	95.4	8	Gonçalves et al., 2021b
$WO_3/CuFe_2O_4$	WCO	180.0	45:1	6.0	3.0	95.2	6	Foroutan et al., 2022
MoO_3/KIT-6	Soybean	150.0	20:1	3.0	3.0	68.51	–	Cardoso et al., 2022
Fe_2O_3-MnO-SO_4/ZrO_2	WCO	180.0	20:1	3.0	6.0	96.0	6	Alhassan et al., 2015
Nb_2O_5/SO_4	Macaw	250.0	120:1	30.0	4.0	99.2	5	Conceição et al., 2016
$Cs_{2.5}PW_{12}O_{40}$	Used vegetable oil	260.0	40:1	3.0	0.67	92.0	–	Shin et al., 2012
MoO_3/Graphene	WCO	140.0	35:1	6.0	5.0	95.6	5	Silva et al., 2023
30-MoO_3/RHA-$CoFe_2O_4$	WFO	160.0	20:1	6.0	3.0	94.6	10	**This study**

which confirms the potential of the 30-MoO_3/RHA-$CoFe_2O_4$ catalyst, as well as indicates that the use of the catalyst can lead to a biodiesel production process with greater economic benefits.

Another important factor to be analyzed is the stability of the catalyst, since this performance affects the process's economy and is a relevant criterion for assessing the suitability of heterogeneous catalysts in industrial applications. Thus, it is worth noting that the data regarding the reuse cycles of the catalysts, presented in Table 4, show that the catalyst developed in this study stands out for its high catalytic stability. The 30-MoO_3/RHA-$CoFe_2O_4$ catalyst can be employed for 10 successive reaction cycles, providing the production of biodiesel with ester contents above 70 %. This represents a considerable advantage when compared to other heterogeneous acidic catalysts, even doubling the catalytic stability exhibited by the majority of the catalysts listed in Table 4. An example of this can be seen in the data concerning the reaction cycles provided by the $HPMo/Nb_2O_5$, $HPMo/TiO_2$, 5Mo/ZSM-22 and Nb_2O_5/SO_4 catalysts.

4. Conclusion

This work studied the application of the new magnetic acid solid catalyst 30-MoO_3/RHA-$CoFe_2O_4$ in the methyl transesterification reaction of WFO for biodiesel synthesis. From the determination of surface acidity, the success of the synthesis method adopted was evidenced. The verification that the catalyst with 30 % molybdenum metal in its composition presented superior catalytic performance was also verified. Through the analysis of XRD, FTIR, SEM, EDS, and VSM, the bifunctional character (catalytic and magnetic) of the synthesized catalyst was verified, which provided the attainment of a biodiesel with 94.6 % ester content under the following optimized reaction conditions: 160.0 °C reaction temperature, methanol:WFO molar ratio of 20:1, catalyst amount of 6.0 wt%, and reaction time of 3.0 h. The catalyst showed ease of separation through the application of a magnetic field and stability over ten reaction cycles. The transesterification reaction also showed chemically controlled behavior and of pseudo first order, according to the kinetic study performed. In short, the 30-MoO_3/RHA-$CoFe_2O_4$ catalyst can be considered promising as a prospect for development and application.

CRediT authorship contribution statement

Matheus Arrais Gonçalves: Conceptualization, Methodology, Investigation, Visualization, Formal analysis, Writing – original draft. **Hiarla Cristina Lima dos Santos:** Methodology, Resources, Investigation. **Thaissa Saraiva Ribeiro:** Methodology, Resources, Investigation. **Alexandre da Cas Viegas:** Methodology, Investigation. **Geraldo Narciso da Rocha Filho:** Supervision. **Leyvison Rafael Vieira da Conceição:** Project administration, Conceptualization, Visualization, Supervision, Project administration, Writing – review & editing.

Declaration of competing interest

The authors declare that they have no known competing financial interests or personal relationships that could have appeared to influence the work reported in this paper.

Acknowledgements

The authors thank the Graduate Program in Chemistry of the Federal University of Pará (UFPA) and the Laboratory of Catalysis and Oleochemical (LCO/UFPA), Research Laboratory and Fuel Analysis (LAPAC/UFPA), X-ray Diffraction Laboratory (PPGF/UFPA), Laboratory of Vibrational Spectroscopy and High Pressures (LEVAP/UFPA) and Metallurgy Laboratory of Federal Institute of Technical Education of Pará for structural support. The Coordenação de Aperfeiçoamento de Pessoal de Nível Superior (CAPES) for the financial support to the author in form of scholarship (finance code 001).

References

Abdullahi, K., Ojonugwa, S.S., Yussuf, A.S., Umaru, M., Mohammed, I.A., Olutoye, M.A., Aberuagba, F., 2023. Optimization of biodiesel production from Allamanda Seed Oil using design of experiment. Fuel Commun. 14, 100081 https://doi.org/10.1016/j.jfueco.2022.100081.

Adhikesavan, C., Ganesh, D., Augustin, V.C., 2022. Effect of quality of waste cooking oil on the properties of biodiesel, engine performance and emissions. Cleaner Eng. Technol. 4, 100070 https://doi.org/10.1016/j.clce.2022.100070.

Alhassan, F.H., Rashid, U., Taufiq-Yap, Y., 2015. Synthesis of waste cooking oil-based biodiesel via effectual recyclable bi-functional Fe_2O_3-MnO-SO_4^{2-}/ZrO_2 nanoparticle solid catalyst. Fuel 142, 38–45. https://doi.org/10.1016/j.fuel.2014.10.038.

Almeida, R.M., Souza, F.T.C., Junior, M.A.C., Alburqueque, N.J.A., Meneghetti, S.M.P., Meneghetti, M.R., 2014. Improvements in acidity for TiO_2 and SnO_2 via impregnation with MoO_3 for the esterification of fatty acids. Catal. Commun. 46, 179–182. https://doi.org/10.1016/j.catcom.2013.12.020.

Asadi, R., Habdollahi, H., Boroumand, Z., Kisomi, A.S., Darvanjooghi, M.H.K., Magdouli, S., Brar, S.K., 2022. Intelligent modelling for the elimination of lanthanides (La^{3+}, Ce^{3+}, Nd^{3+} and Eu^{3+}) from aqueous solution by magnetic $CoFe_2O_4$ and $CoFe_2O_4$-GO spinel ferrite nanocomposites. Environ. Pollut. 309, 119770 https://doi.org/10.1016/j.envpol.2022.119770.

Ashok, A., Kennedy, L.J., 2019. Magnetically separable zinc ferrite nanocatalyst for an efective biodiesel production from waste cooking oil. Catal. Lett. 119, 3525–3542. https://doi.org/10.1007/s10562-019-02906-4.

Atta, A.Y., Jibril, B.Y., Aderemi, B.O., Adefila, S.S., 2012. Preparation of analcime from local kaolin and rice husk ash. Appl. Clay Sci. 61, 8–13. https://doi.org/10.1016/j.clay.2012.02.018.

Aziz, M.M.A., Puad, K., Triwahyono, S., Jalil, A.A., Khayoon, M.S., Atabani, A.E., Ramli, Z., Majid, Z.A., Prasetyoko, D., Hartanto, D., 2017. Transesterification of croton megalocarpus oil to biodiesel over WO_3 supported on sílica mesoporous-macroparticles catalyst. Chem. Eng. Journ. 316, 882–892. https://doi.org/10.1016/j.cej.2017.02.049.

Bastos, R.R.C., Correa, A.P.L., da Luz, P.T.S., Filho, G.N.R., Zamian, J.R., Conceição, L.R.V., 2020. Optimization of biodiesel production using sulfonated carbon-based catalyst from an amazon agro-industrial waste. Energ. Convers. Manage. 205, 112457 https://doi.org/10.1016/j.enconman.2019.112457.

Beall, H., 1994. Probing student misconceptions in thermodynamics with in-class writing. J. Chem. Educ. 71, 1056–1057.

Boehm, H.P., 1994. Some aspects of the surface chemistry of carbon blacks and other carbons. Carbon 32, 759–769. https://doi.org/10.1016/0008-6223(94) 90031-0.

Caliman, E., Dias, J.A., Dias, S.C.L., Garcia, F.A.C., de Macedo, J.L., Almeida, L.S., 2010. Preparation and characterization of $H_3PW_{12}O_{40}$ supported on niobia. Microporous Mesoporous Mater. 132, 103–111. https://doi.org/10.1016/j.micromeso.2010.02.004.

Cardoso, R.K.P., Silva, G.V.A., Alves, B.T.S., Freire, V.A., Alves, J.J.N., Barbosa, B.V.S., 2022. Evaluation of the effect of Si/Mo and oil/alcohol ratios in the production of biodiesel from soybean oil. Arabian J. Chem. 15, 104074 https://doi.org/10.1016/j.arabjc.2022.104074.

Chen, G.Y., Shan, R., Shi, J.F., Yan, B.B., 2015. Transesterification of palm oil to biodiesel using rice husk ash-based catalysts. Fuel Process. Technol. 133, 8–13. https://doi.org/10.1016/j.fuproc.2015.01.005.

Chen, K.T., Wang, J.X., Dai, Y.M., Wang, P.H., Liou, C.Y., Nien, C.W., Wu, J.S., Chen, C. C., 2013. Rice husk ash as a catalyst precursor for biodiesel production. J. Taiwan Inst. Chem. Eng. 44, 622–629. https://doi.org/10.1016/j.jtice.2013.01.006.

Conceição, L.R.V., Carneiro, L.M., Rivaldi, J.D., De Castro, H.F., 2016. Solid acid as catalyst for biodiesel production via simultaneous esterification and transesterification of macaw palm oil. Ind. Crop. Prod. 89, 416–424. https://doi.org/10.1016/j.indcrop.2016.05.044.

Conceição, L.R.V., Carneiro, L.M., Giordani, D.S., de Castro, H.F., 2017. Synthesis of biodiesel from macaw palm oil using mesoporous solid catalyst comprising 12-molybdophosphoric acid and niobia. Renew. Energy 113, 119–128. https://doi.org/10.1016/j.renene.2017.05.080.

Conceição, L.R.V., Reis, C.E.R., de Lima, R., Cortez, D.V., De Castro, H.F., 2019. Keggin-structure heteropolyacid supported on alumina to be used in trans/esterification of high acid feedstocks. RSC Adv. 9, 23450–23458. https://doi.org/10.1039/C9RA04300D.

Correa, A.P.L., Bastos, R.R.C., Filho, G.N.R., Zamian, J.R., Conceição, L.R.V., 2020. Preparation of sulfonated carbon-based catalysts from murumuru kernel shell and their performance in the esterification reaction. RSC Adv. 10, 20245–20256. https://doi.org/10.1039/DORA03217D.

Correa, A.P.L., Silva, P.M.L., Gonçalves, M.A., Bastos, R.R.C., Filho, G.N.R., Conceição, L. R.V., 2023. Study of the activity and stability of sulfonated carbon catalyst from agroindustrial waste in biodiesel production: Influence of pyrolysis temperature on functionalization. Arabian J. Chem. 16, 104964 https://doi.org/10.1016/j.arabjc.2023.104964.

Dhage, S.R., Hassan, M.S., Yang, O.-B., 2009. Low temperature fabrication of hexagon shaped h-MoO_3 nanorods and its phase transformation. Mat. Chem. Phys. 114, 511–514. https://doi.org/10.1016/j.matchemphys.2008.10.076.

Dos Santos, H.C.L., Gonçalves, M.A., Viegas, A.C., Figueira, B.A.M., Luz, P.T.S., Filho, G. N.R., Conceição, L.R.V., 2022. Tungsten oxide supported on copper ferrite: a novel magnetic acid heterogeneous catalyst for biodiesel production from low quality feedstock. RSC Adv. 12, 34614. https://doi.org/10.1039/d2ra06923g.

Erison, A.E.A., Tan, Y.H., Mubarak, N.M., Kansedo, J., Khalid, M., Abdullah, M.O., Ghasemi, M., 2022. Life cycle assessment of biodiesel production by using impregnated magnetic biochar derived from waste palm kernel shell. Environ. Res. 214, 114149 https://doi.org/10.1016/j.envres.2022.114149.

Foroutan, R., Peighambardoust, S.J., Mohammadi, R., Peighambardoust, S.H., Ramavandi, B., 2022. Application of waste chalk/$CoFe_2O_4$/K_2CO_3 composite as a reclaimable catalyst for biodiesel generation from sunflower oil. Chemosphere 289, 133226. https://doi.org/10.1016/j.chemosphere.2021.133226.

Gardy, J., Osatiashtiani, A., Cespedes, O., Hassanpour, A., Lai, X., Lee, A.F., Wilson, K., Rehan, M., 2018. A magnetically separable SO_4/Fe-Al-TiO_2 solid catalyst for biodiesel production from waste cooking oil. Appl. Catal. b. 234, 268–278. https://doi.org/10.1016/j. apcatb.2018.04.046.

Gonçalves, M.A., Mares, E.K.L., Luz, P.T.S., Zamian, J.R., Filho, G.N.R., Castro, H.F., Conceição, L.R.V., 2021a. Biodiesel synthesis from waste cooking oil using heterogeneous acid catalyst: Statistical optimization using linear regression model. J. Renew. Sustain. Energy 13, 043101. https://doi.org/10.1063/5.0048147.

Gonçalves, M.A., Mares, E.K.L., Zamian, J.R., Filho, G.N.R., Conceição, L.R.V., 2021b. Statistical optimization of biodiesel production from waste cooking oil using magnetic acid heterogeneous catalyst MoO_3/$SrFe_2O_4$. Fuel 304, 121463. https://doi.org/10.1016/j.fuel.2021.121463.

Helmiyati, H., Suci, R.P., 2019. Nanocomposite of cellulose-ZnO/SiO_2 as catalyst biodiesel methyl ester from virgin coconut oil. AIP Conf. Proc. 2168, 020063 https://doi.org/10.1063/1.5132490.

Jayalakshmi, R., Jeyanthi, J., 2018. Synthesis and structural characterization of polymer-based cobalt ferrite nanocomposite with core-shell structure. J. Inorg. Organomet. Polym. Mater. 28, 1286–1293. https://doi.org/10.1007/s10904-018-0821-z.

Kaur, M., Malhotra, R., Ali, A., 2018. Tungsten supported Ti/SiO_2 nanoflowers as reusable heterogeneous catalyst for biodiesel production. Renew. Energy 116, 109–119. https://doi.org/10.1016/j.renene.2017.09.065.

Kiehbadroudinezhad, M., Merabet, A., Hosseinzadeh-Bandbafha, H., 2023. A life cycle assessment perspective on biodiesel production from fish wastes for green microgrids in a circular bioeconomy. Bioresour. Technol. Rep 21, 101303. https://doi.org/10.1016/j.biteb.2022.101303.

Krishnan, S.G., Pua, F., Zhang, F., 2021. A review of magnetic solid catalyst development for sustainable biodiesel production. Biomass Bioener. 149, 106099 https://doi.org/10.1016/j.biombioe.2021.106099.

Kumar, P.R., Kollu, P., Santhosh, S., Rao, K.E.V., Kim, D.K., Grace, A.N., 2014. Enhanced properties of porous $CoFe_2O_4$–reduced graphene oxide composites with alginate binders for Li-ion battery applications. New J. Chem. 38, 3654. https://doi.org/10.1039/c4nj00419a.

Lima, R.P., Luz, P.T.S., Braga, M., Santos, P.R., Costa, C.E.F., Zamian, J.R., Nascimento, L.A.S., Filho, G.N.R., 2017. Murumuru (Astrocaryum murumuru Mart.) butter and oils of buriti (Mauritia flexuosa Mart.) and pracaxi (Pentaclethra macroloba (Willd.) Kuntze) can be used for biodiesel production: Physico-chemicalproperties and thermal and kinetic studies. Ind. Crop. Prod. 97, 536–544. https://doi.org/10.1016/j.indcrop.2016.12.052.

Liu, S.T., Chen, X.G., Zhang, A.B., Yan, K.K., Ye, Y., 2014. Electromagnetic performance of rice husk ash. Bioresources 9, 2328–2340.

Ma, Q., Li, X., Li, G., Shao, Z., 2020. Synthesis and electrochemical performance of MoO_3 anode material prepared by polymer network gel method. Ionics 27, 157–164. https://doi.org/10.1007/s11581-020-03824-x.

Mares, E.K.L., Gonçalves, M.A., Luz, P.T.S., Filho, G.N.R., Zamian, J.R., Conceição, L.R. V., 2021. Acai seed ash as novel basic heterogeneous catalyst for biodiesel synthesis: optimization of the biodiesel production process. Fuel 299, 120887. https://doi.org/10.1016/j.fuel.2021.120887.

Mawlid, O.A., Abdelhady, H.H., El-Deab, M.S., 2022. Boosted biodiesel production from waste cooking oil using novel SrO/$MgFe_2O_4$ magnetic nanocatalyst at low temperature: Optimization process. Energ. Convers. Manag. 273, 116435 https://doi.org/10.1016/j.enconman.2022.116435.

Mehrabadi, B.A.T., Eskandari, S., Khan, U., White, R.D., Regalbuto, J.R., 2017. A review of preparation methods for supported metal catalysts. Adv. Catal. 61, 1–35. https://doi.org/10.1016/bs.acat.2017.10.001.

Moayedi, H., Aghel, B., Abdullahi, M.M., Nguyen, H., Rashid, A.S.A., 2019. Applications of rice husk ash as green and sustainable biomass. J. Clean. Prod. 237, 117851 https://doi.org/10.1016/j.jclepro.2019.117851.

Mohebbi, S., Rostamizadeh, M., Kahforoushan, D., 2020. Effect of molybdenum promoter on performance of high silica MoO_3/B-ZSM-5 nanocatalyst in biodiesel production. Fuel 266, 117063. https://doi.org/10.1016/j.fuel.2020.117063.

Oliveira, A.N., Lima, M.A.B., Pires, L.H.O., Silva, M.S., Da Silva, P.T.S., Angelica, R.S., Filho, G.N.R., Costa, C.E.F., Luque, R., Nascimento, L.A.S., 2019. Bentonites modified with phosphomolybdic heteropolyacid (HPMo) for biowaste to biofuel production. Materials 12, 1431. https://doi.org/10.3390/ma12091431.

Olubunmi, B.E., Alade, A.F., Ebhodaghe, S.O., Oladapo, O.T., 2022. Optimization and kinetic study of biodiesel production from beef tallow using calcium oxide as a heterogeneous and recyclable catalyst. Energ. Convers. Manag: X 14, 10022. https://doi.org/10.1016/j.ecmx.2022.100221.

Parrillo, A., Sanchez, G., Alles, A.B., 2021. α-Si_3N_4 and Si_2N_2O whiskers from rice husk and industrial rice husk ash. SN Applied Sciences 3, 268. https://doi.org/10.1007/s42452-021-04307-y.

Pinto, B.F., Garcia, M.A.S., Costa, J.C.S., Moura, C.R.V., Abreu, W.C., Moura, E.M., 2019. Effect of calcination temperature on the application of molybdenum trioxide acid catalyst: Screening of substrates for biodiesel production. Fuel 239, 290–296. https://doi.org/10.1016/j.fuel.2018.11.025.

Racik, K.M., Anand, S., Muniyappan, S., Nandhini, S., Rameshkumar, S., Mani, D., Karuppasamy, P., Pandian, M.S., Ramasamy, P., 2022. Preparation of $CoFe_2O_4$/SiO_2 nanocomposite as potential electrode materials for supercapacitors. Inorg. Chem. Commun. 146, 110036 https://doi.org/10.1016/j.inoche.2022.110036.

Shi, M., Zhang, P.B., Fan, M.M., Jiang, P.P., Dong, Y.M., 2017. Influence of crystal of Fe_2O_3 in magnetism and activity of nanoparticle CaO@Fe_2O_3 for biodiesel production. Fuel 197, 343–347. https://doi.org/10.1016/j.fuel.2017.02.060.

Shin, H.Y., An, S.H., Sheikh, R., Park, Y.H., Bae, S.Y., 2012. Transesterification of used vegetable oils with a Cs-doped heteropolyacid catalyst in supercritical methanol. Fuel 96, 572–578. https://doi.org/10.1016/j.fuel.2011.12.076.

Silva, P.M.M., Gonçalves, M.A., Corrêa, A.P.L., Luz, P.T.S., Zamian, J.R., Filho, G.N.R., Conceição, L.R.V., 2023. Preparation and characterization of a novel efficient catalyst based on molybdenum oxide supported over graphene oxide for biodiesel synthesis. Renew. Energy 211, 126–139. https://doi.org/10.1016/j.renene.2023.04.131.

Tamjidi, S., Moghadas, B.K., Esmaeili, H., 2022. Ultrasound-assisted biodiesel generation from waste edible oil using $CoFe_2O_4$@GO as a superior and reclaimable nanocatalyst: Optimization of two-step transesterification by RSM. Fuel 327, 125170. https://doi.org/10.1016/j.fuel.2022.125170.

Tang, S.K., Wang, L.P., Zhang, Y., Li, S.F., Tian, S.J., Wang, B.Y., 2012. Study on preparation of Ca/ Al/Fe_3O_4 magnetic composite solid catalyst and its application in biodiesel transesterification. Fuel Process Technol 95, 84–89. https://doi.org/10.1016/j.fuproc.2011.11.022.

Thangasamy, P., Shanmugapriya, V., Sathish, M., 2018. One-dimensional growth of hexagonal rods of metastable h-MoO_3 using one-pot, rapid and environmentally benign supercritical fluid processing. Physica e: Low-Dimens. Syst. Nanostruct. 99, 189–193. https://doi.org/10.1016/j.physe.2018.02.001.

Ulakpa, W.C., Ulakpa, R.O.E., Eyankware, E.O., Egwunyenga, M.C., 2022. Statistical optimization of biodiesel synthesis from waste cooking oil using NaOH/ bentonite impregnated catalyst. Cleaner Waste Syst. 3, 100049 https://doi.org/10.1016/j.clwas.2022.100049.

Wang, Y.T., Yang, X.X., Xu, J., Wang, H.L., Wang, Z.B., Zhang, L., Wang, S.L., Liang, J.L., 2019. Biodiesel production from esterification of oleic acid by a sulfonated magnetic solid acid catalyst. Renew. Energy 139, 688–695. https://doi.org/10.1016/j.renene.2019.02.111.

Xie, W., Li, J., 2023. Magnetic solid catalysts for sustainable and cleaner biodiesel production: a comprehensive review. Renew. Sustain. Energy Rev. 171, 113017 https://doi.org/10.1016/j.rser.2022.113017.

Zhang, W., Wang, C., Luo, B., He, P., Zhang, L., Hu, G., 2022. Efficient and economic transesterification of waste cooking soybean oil to biodiesel catalyzed by outer surface of ZSM-22 supported different Mo catalyst. Biomass Bioenergy 167, 106646. https://doi.org/10.1016/j.biombioe.2022.106646.